6

Global Food Security Support Analysis Data at Nominal 1 km (GFSAD1km) Derived from Remote Sensing in Support of Food Security in the Twenty-First Century: Current Achievements and Future Possibilities

Pardhasaradhi Teluguntla
U.S. Geological Survey
and
Bay Area Environmental Research Institute

Prasad S. Thenkabail
U.S. Geological Survey

Jun Xiong
U.S. Geological Survey
and
Northern Arizona University

Murali Krishna Gumma
International Crops Research Institute for the Semi Arid Tropics

Chandra Giri
U.S. Geological Survey, (EROS) Center

Cristina Milesi
NASA Ames Research Center

Mutlu Ozdogan
University of Wisconsin

Russell G. Congalton
University of New Hampshire

James Tilton
NASA Goddard Space Flight Center

Temuulen Tsagaan Sankey
Northern Arizona University

Richard Massey
Northern Arizona University

Aparna Phalke
University of Wisconsin

Kamini Yadav
University of New Hampshire

Acronyms and Definitions

ACCA	Automated cropland classification algorithm
ASTER	Advanced spaceborne thermal emission and reflection radiometer
AVHRR	Advanced very-high-resolution radiometer
AWiFS	Advanced wide field sensor
CDL	The Cropland Data Layer (CDL) was created by the USDA, National Agricultural Statistics Service
CEOS	Committee on Earth Observing Satellites (CEOS)
EDS	Euclidean distance similarity
FPA	Full pixel areas
GCAD	Global cropland area database
GCE	Global cropland extent
GCE V1.0	Global cropland extent version 1.0
GDEM	ASTER-derived digital elevation data
GEO	Group on Earth Observations
GEOSS	Global Earth Observation System of Systems
GFSAD	Global food security support analysis data
GIMMS	Global Inventory Modeling and Mapping Studies
JERS SAR	Japanese Earth Resources Satellite-1 (JERS-1)
ISDB IA	Ideal Spectra Data Bank on Irrigated Areas
LEDAPS	Landsat Ecosystem Disturbance Adaptive Processing System
MFDC	Mega File Data Cube
MODIS	Moderate-resolution imaging spectroradiometer
MSAS	Modified spectral angle similarity
NASS	National Agricultural Statistics Service of USDA
NDVI	Normalized difference vegetation index
NOAA	National Oceanic and Atmospheric Administration
SAR	Synthetic aperture radar
SCS	Spectral correlation similarity
SIT	Strategic Implementation Team
SMT	Spectral matching techniques
SPA	Subpixel areas
SPOT	Système Pour l'Observation de la Terre
SSV	Spectral similarity value
USDA	United States Department of Agriculture
USGS	United States Geological Survey
VGT	Vegetation sensor of SPOT satellite
VHRI	Very-high-resolution imagery
VHRR	Very-high-resolution radiometer

6.1 Introduction

The precise estimation of the global agricultural cropland—extents, areas, geographic locations, crop types, cropping intensities, and their watering methods (irrigated or rain-fed; type of irrigation)—provides a critical scientific basis for the development of water and food security policies (Thenkabail et al., 2010, 2011, 2012, Turral et al., 2009). By year 2100, the global human population is expected to grow to 10.4 billion under median fertility variants or higher under constant or higher fertility variants (Table 6.1) with over three-quarters living in developing countries and in regions that already lack the capacity to produce enough food. With current agricultural practices, the increased demand for food and nutrition would require about 2 billion hectares of additional cropland, about twice the equivalent to the land area of the United States, and lead to significant increases in greenhouse gas emissions (GHG) associated with agricultural practices and activities (Tillman et al., 2011). For example, during 1960–2010, world population more than doubled from 3 to 7 billion. The nutritional demand of the population also grew swiftly during this period from an average of about 2000 calories per day per person in 1960 to nearly 3000 calories per day per person in 2010. The food demand of increased population along with increased nutritional demand during this period was met by the "green revolution," which more than tripled the food production, even though croplands decreased from about 0.43 ha per capita to 0.26 ha per capita (FAO, 2009; Funk and Brown, 2009). The increase in food production during the green revolution was the result of factors such as: (1) expansion of irrigated croplands, which had increased in 2000 from 130 Mha in the 1960s to between 278 Mha (Siebert et al., 2006) and 467 Mha (Thenkabail et al., 2009a,b,c), with the larger estimate due to consideration of cropping intensity; (2) increase in yield and per capita production of food (e.g., cereal production from 280 to 380 kg/person and meat from 22 to 34 kg/person (McIntyre, 2008); (3) new cultivar types (e.g., hybrid varieties of wheat and rice, biotechnology); and (4) modern agronomic and crop management practices (e.g., fertilizers, herbicide, pesticide applications).

Although modern agriculture met the challenge to increase food production last century, lessons learned from the twentieth century "green revolution" and our current circumstances impact the likelihood of another such revolution. The intensive

TABLE 6.1 World Population (Thousands) Under All Variants, 1950–2100

Year	Medium Fertility Variant	High Fertility Variant	Low Fertility Variant	Constant Fertility Variant
1950	2,529,346	2,529,346	2,529,346	2,529,346
1955	2,763,453	2,763,453	2,763,453	2,763,453
1960	3,023,358	3,023,358	3,023,358	3,023,358
1965	3,331,670	3,331,670	3,331,670	3,331,670
1970	3,685,777	3,685,777	3,685,777	3,685,777
1975	4,061,317	4,061,317	4,061,317	4,061,317
1980	4,437,609	4,437,609	4,437,609	4,437,609
1985	4,846,247	4,846,247	4,846,247	4,846,247
1990	5,290,452	5,290,452	5,290,452	5,290,452
1995	5,713,073	5,713,073	5,713,073	5,713,073
2000	6,115,367	6,115,367	6,115,367	6,115,367
2005	6,512,276	6,512,276	6,512,276	6,512,276
2010	6,916,183	6,916,183	6,916,183	6,916,183
2015	7,324,782	7,392,233	7,256,925	7,353,522
2020	7,716,749	7,893,904	7,539,163	7,809,497
2025	8,083,413	8,398,226	7,768,450	8,273,410
2030	8,424,937	8,881,519	7,969,407	8,750,296
2035	8,743,447	9,359,400	8,135,087	9,255,828
2040	9,038,687	9,847,909	8,255,351	9,806,383
2045	9,308,438	10,352,435	8,323,978	10,413,537
2050	9,550,945	10,868,444	8,341,706	11,089,178
2055	9,766,475	11,388,551	8,314,597	11,852,474
2060	9,957,399	11,911,465	8,248,967	12,729,809
2065	10,127,007	12,442,757	8,149,085	13,752,494
2070	10,277,339	12,989,484	8,016,514	14,953,882
2075	10,305,146	13,101,094	7,986,122	15,218,723
2080	10,332,223	13,213,515	7,954,481	15,492,520
2085	10,358,578	13,326,745	7,921,618	15,775,624
2090	10,384,216	13,440,773	7,887,560	16,068,398
2095	10,409,149	13,555,593	7,852,342	16,371,225
2100	10,433,385	13,671,202	7,815,996	16,684,501

Source: UNDP, *Human Development Report 2012: Overcoming Barriers: Human Mobility and Development*, New York, United Nations, 2012.

use of chemicals has adversely impacted the environment in many regions, leading to salinization and decreasing water quality and degrading croplands. From 1960 to 2000, worldwide phosphorous use doubled from 10 million tons (MT) to 20 MT, pesticide use tripled from near zero to 3 MT, and nitrogen use as fertilizer increased to a staggering 80 MT from just 10 MT (Foley et al., 2007; Khan and Hanjra, 2008). Diversion of croplands to biofuels is taking water away from food production (Bindraban et al., 2009), even as the economic, carbon sequestration, environmental, and food security impacts of biofuel production are proving to be a net negative (Gibbs et al., 2008; Lal and Pimentel, 2009; Searchinger et al., 2008). Climate models predict that the hottest seasons on record will become the norm by the end of the century in most regions of the world—a prediction that bodes ill for feeding the world (Kumar and Singh, 2005). Increasing per capita meat consumption is increasing agricultural demands on land and water (Vinnari and Tapio, 2009). Cropland areas are decreasing in many parts of the world due to urbanization, industrialization, and salinization (Khan and Hanjra, 2008). Ecological and environmental imperatives, such as biodiversity conservation and atmospheric carbon sequestration, have put a cap on the possible expansion of cropland areas to other lands such as forests and rangelands (Gordon et al., 2009). Crop yield increases of the green revolution era have now stagnated (Hossain et al., 2005). Given these factors and limitations, further increase in food production through increase in cropland areas and/or increased allocations of water for croplands is widely considered unsustainable or simply infeasible.

Clearly, our continued ability to sustain adequate global food production and achieve future food security in the twenty-first century is challenged. So, how does the world continue to meet its food and nutrition needs? Solutions may come from biotechnology and precision farming. However, developments in these fields are not currently moving at rates that will ensure global food security over the next few decades (Foley et al., 2011). Further, there is a need for careful consideration of possible adverse effects of biotechnology. We should not be looking back 30–50 years from now with regrets, like we are looking back now at many mistakes made during the green revolution. During the green revolution, the focus was only on getting more yield per unit area. Little thought was given to the serious damage done to our natural environments, water resources, and human health as a result of detrimental factors such as uncontrolled use of herbicides, pesticides, and nutrients, drastic groundwater mining, and salinization of fertile soils due to overirrigation. Currently, there are discussions of a "second green revolution" or even an "evergreen revolution," but definitions of what these terms actually mean are still debated and are evolving (e.g., Monfreda et al., 2008). One of the biggest issues that has not been given adequate focus is the use of large quantities of water for food production. Indeed, an overwhelming proportion (60%–90%) of all human water use in the World, for example, goes for producing their food (Falkenmark and Rockström, 2006). But such intensive water use for food production is no longer sustainable due to increasing competition for water in alternative uses (EPW, 2008), such as urbanization, industrialization, environmental flows, biofuels, and recreation. This has brought into sharp focus the need to grow more food per drop of water (or crop water productivity or crop per drop) leading to the need for a "blue revolution" in agriculture (Pennisi, 2008).

A significant part of the solution lies in determining how global croplands are currently used and how they might be better managed to optimize the use of resources in food production. This will require development of an advanced global cropland area database (GCAD) with an ability to map global croplands and their attributes routinely, rapidly, consistently, and with sufficient accuracies. This in turn

requires the creation of a framework of best practices for cropland mapping and an advanced global geospatial information system on global croplands. Such a system would need to be consistent across nations and regions by providing information on issues such as the composition and location of cropping, cropping intensities (e.g., single, double crop), rotations, crop health/vigor, and irrigation status. Opportunities to establish such a global system can be achieved by fusing advanced remote sensing data from multiple platforms and agencies (e.g., http://eros.usgs.gov/ceos/satellites_midres1.shtml; http://www.ceos-cove.org/index.php) in combination with national statistics, secondary data (e.g., elevation, slope, soils, temperature, and precipitation), and the systematic collection of field level observations. An example of such a system on a regional scale is USDA, NASS Cropland Data Layer (CDL), which is a raster, georeferenced, crop-specific land cover data layer with a ground resolution of 30 m (Johnson and Mueller, 2010). The GCAD will be a major contribution to Group on Earth Observations (GEO) Global Agricultural Monitoring Initiative (GLAM), to the overarching vision of GEO Agriculture and Water Societal Beneficial Areas (GEO Ag. SBAs), G20 Agriculture Ministers initiatives, and ultimately to the Global Earth Observation System of Systems (GEOSS). These initiatives are also supported by the Committee on Earth Observing Satellites (CEOS) Strategic Implementation Team (SIT).

Within the context of the above facts, the overarching goal of this chapter is to provide a comprehensive overview of the state-of-art of global cropland mapping procedures using remote sensing as characterized and envisioned by the "Global Food Security Support Analysis Data @ 30 m (GFSAD30)" project working group team. First, the chapter will provide an overview of *existing cropland maps* and their characteristics along with establishing the gaps in knowledge related to global cropland mapping. Second, *definitions* of cropland mapping along with key parameters involved in cropland mapping based on their importance in food security analysis, and cropland naming conventions for standardized cropland mapping using remote sensing will be presented. Third, *existing methods and approaches* for cropland mapping will be discussed. This will include the type of remote sensing data used in cropland mapping and their characteristics along with discussions on the secondary data, field-plot data, and cropland mapping algorithms. Fourth, currently *existing global cropland products* derived using remote sensing will be presented and discussed. Fifth, a *synthesis* of all existing products leading to a composite global cropland extent version 1.0 (GCE V1.0) is presented and discussed. Sixth, a *way forward* for advanced global cropland mapping is visualized.

6.2 Global Distribution of Croplands and Other Land Use and Land Cover: Baseline for the Year 2000

The first comprehensive global map of croplands was created by Ramankutty et al. in 1998. A more current version for the year 2000 shows the spatial distribution of global croplands along with other land use and land cover classes (Figure 6.1). This provides a first view of where global croplands are concentrated and helps us to focus on the appropriate geographic locations for detailed cropland studies. Water and snow (Class 8 and 9, respectively) have zero croplands and occupy 44% of the total terrestrial land surface. Further, forests (Class 6) occupy 17% of the terrestrial area and deserts (Class 7) an additional 12%. In these two classes, <5% of the total croplands exist. Therefore, in order to study croplands systematically and intensively, one must prioritize mapping in the areas of Classes 1–5 (26% of the terrestrial area) where >95% of all global croplands exist, with the first 3 classes (Class 1, 2, and 3) having ~75% and the next 2 ~20%. In the future, it is likely some of the noncroplands may be converted to croplands (e.g., especially in Africa where large farmlands are introduced in recent years in otherwise overwhelmingly small-holder dominant farming) or vice versa, highlighting the need for repeated and systematic global mapping of croplands. Segmenting the world into cropland versus noncropland areas routinely will help us understand and study these change dynamics better.

6.2.1 Existing Global Cropland Maps: Remote Sensing and Non–Remote Sensing Approaches

There are currently six major global cropland maps: (1) Thenkabail et al. (2009a,b), (2) Ramankutty and Foley (1998), (3) Goldewijk et al. (2011), (4) Portmann et al. (2010), (5) Pittman et al. (2010), and (6) Yu et al. (2013). These studies estimated the total global cropland area to be around 1.5 to 1.7 billion hectares for the year 2000 as a baseline. However, there are two significant differences in these products: (1) spatial disagreement on where the actual croplands are, and (2) irrigated to rain-fed cropland proportions and their precise spatial locations. Globally, cropland areas have increased from around 265 Mha in year 1700 to around 1471 Mha in year 1990, while the area of pasture has increased approximately sixfold from 524 to 3451 Mha (Foley et al., 2011). Ramankutty and Foley (1998) estimated the cropland and pasture to represent about 36% of the world's terrestrial surface (148,940,000 km^2), of which, according to different studies, roughly 12% is croplands and 24% pasture. Multiple studies (Goldewijk et al., 2011; Portmann et al., 2010; Ramankutty et al., 2008) integrated agricultural statistics and census data from the national systems with spatial mapping technologies involving geographic information systems (GIS) to derive global cropland maps.

Thenkabail and others (2009a,b, 2011) produced the first remote sensing–based global irrigated and rain-fed cropland maps and statistics through multisensor remote sensing data fusion along with secondary data and in situ data. They further used five dominant crop types (wheat, rice, corn, barley, and soybeans) using parcel-based inventory data (Monfreda et al., 2005, 2008; Portmann et al., 2010; Ramankutty et al., 2008) to produce a classification of global croplands with crop dominance (Thenkabail et al., 2012). The five crops account for about 60% of the total global cropland

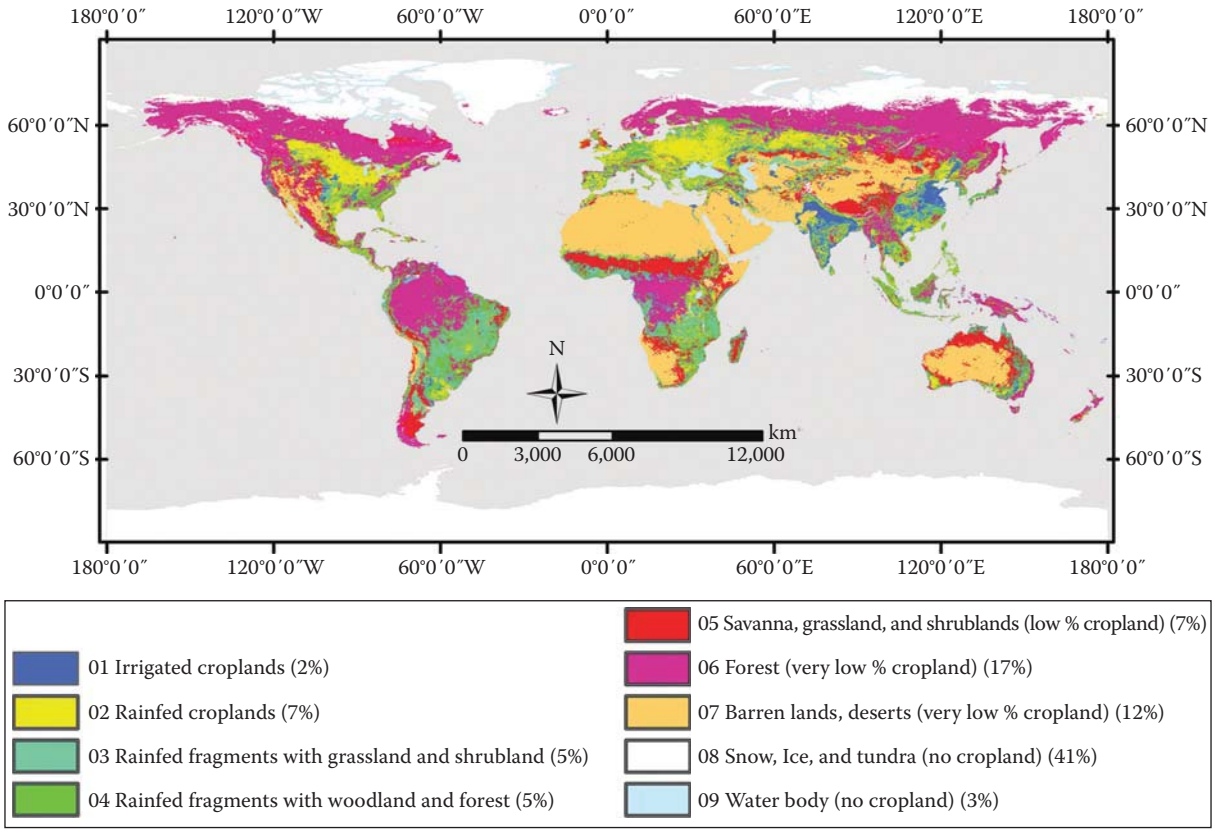

FIGURE 6.1 Global croplands and other land use and land cover: Baseline.

areas. The precise spatial location of these crops is only an approximation due to the coarse resolution (approximately 1 km^2) and fractional representation (1%–100% crop in a pixel) of the crop data in each grid cell of all the maps from which this composite map is produced (Thenkabail et al., 2012). The existing global cropland datasets also differ from each other due to inherent uncertainties in establishing the precise location of croplands, the watering methods (rain-fed versus irrigated), cropping intensities, crop types and/or dominance, and crop characteristics (e.g., crop or water productivity measures such as biomass, yield, and water use). Improved knowledge of the uncertainties (Congalton and Green, 2009) in these estimates will lead to a suite of highly accurate spatial data products (Goodchild and Gopal, 1989) in support of crop modeling, food security analysis, and decision support.

6.3 Key Remote Sensing–Derived Cropland Products: Global Food Security

The production of a repeatable global cropland product requires a standard set of metrics and attributes that can be derived consistently across the diverse cropland regions of the world. Four key cropland information systems attributes that have been identified for global food security analysis and that can be readily derived from remote sensing include (Figure 6.2): (1) cropland extent/areas, (2) watering methods (e.g., irrigated, supplemental irrigated, and rain-fed), (3) crop types, and (4) cropping intensities (e.g., single crop, double crop, and continuous crop). Although not the focus of this chapter, many other parameters are also derived in local regions, such as: (5) precise location of crops, (6) cropping calendar, (7) crop health/vigor, (8) flood and drought information, (9) water use assessments, and (10) yield or productivity (expressed per unit of land and/or unit of water). Remote sensing is specifically suited to derive the four key products over large areas using fusion of advanced remote sensing (e.g., Landsat, Resourcesat, MODIS) in combination with national statistics, ancillary data (e.g., elevation, precipitation), and field-plot data. Such a system, at the global level, will be complex in data handling and processing and requires coordination between multiple agencies leading to development of a seamless, scalable, transparent, and repeatable methodology. As a result, it is important to have a systematic class labeling convention as illustrated in Figure 6.3. A standardized class identifying and labeling process (Figure 6.3) will enable consistent and systematic labeling of classes, irrespective of analysts. First, the area is separated into cropland versus noncropland. Then, within the cropland class, labeling will involve (Figure 6.3): (1) cropland extent (cropland versus noncropland), (2) watering source (e.g., irrigated versus rain-fed), (3) irrigation source (e.g., surface water, ground water), (4) crop type or dominance, (5) scale (e.g., large or contiguous, small or fragmented), and (6) cropping intensity (e.g., single crop, double crop). The detail at which one maps at each stage and each

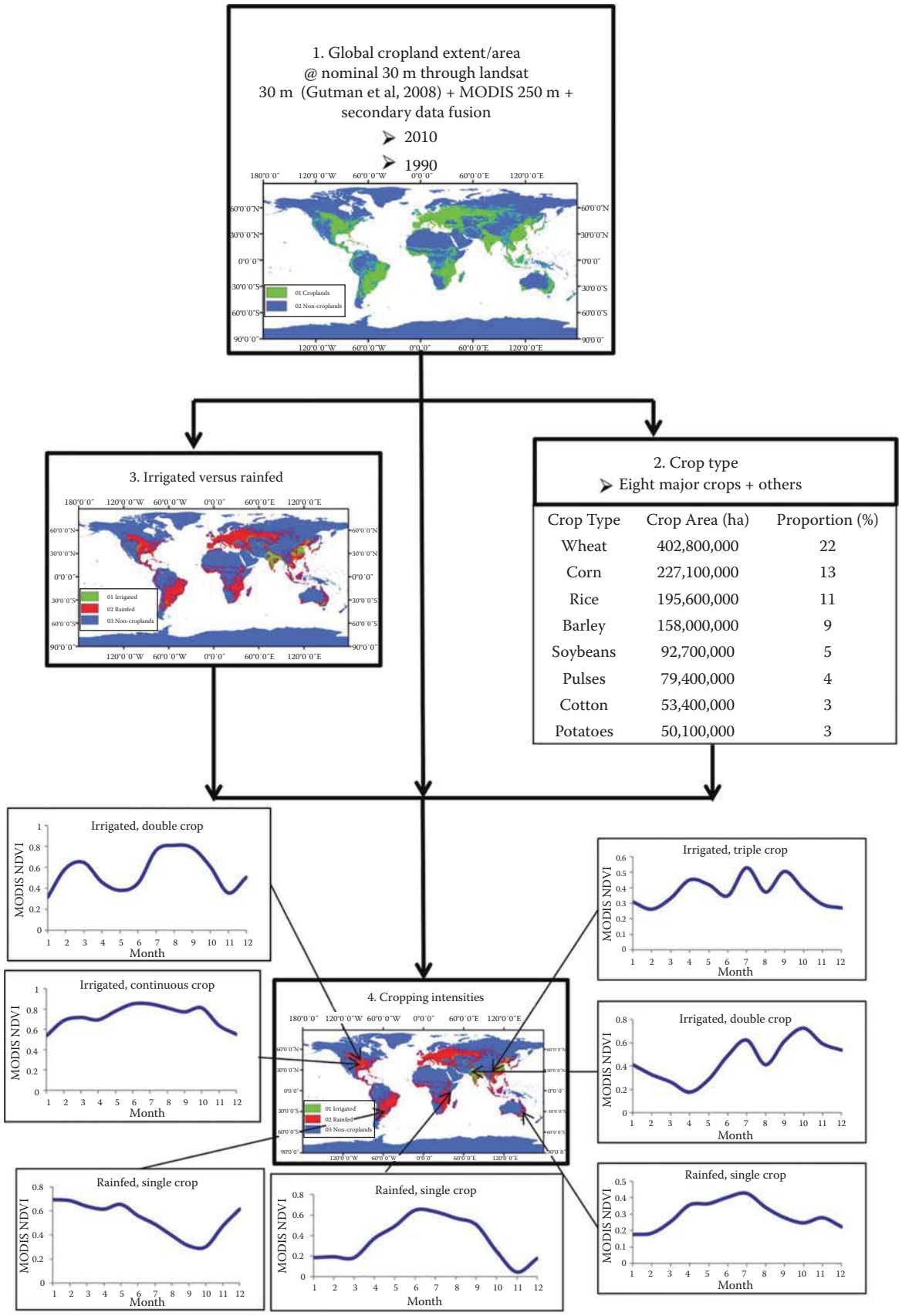

FIGURE 6.2 Key global cropland area products that will support food security analysis in the twenty-first century.

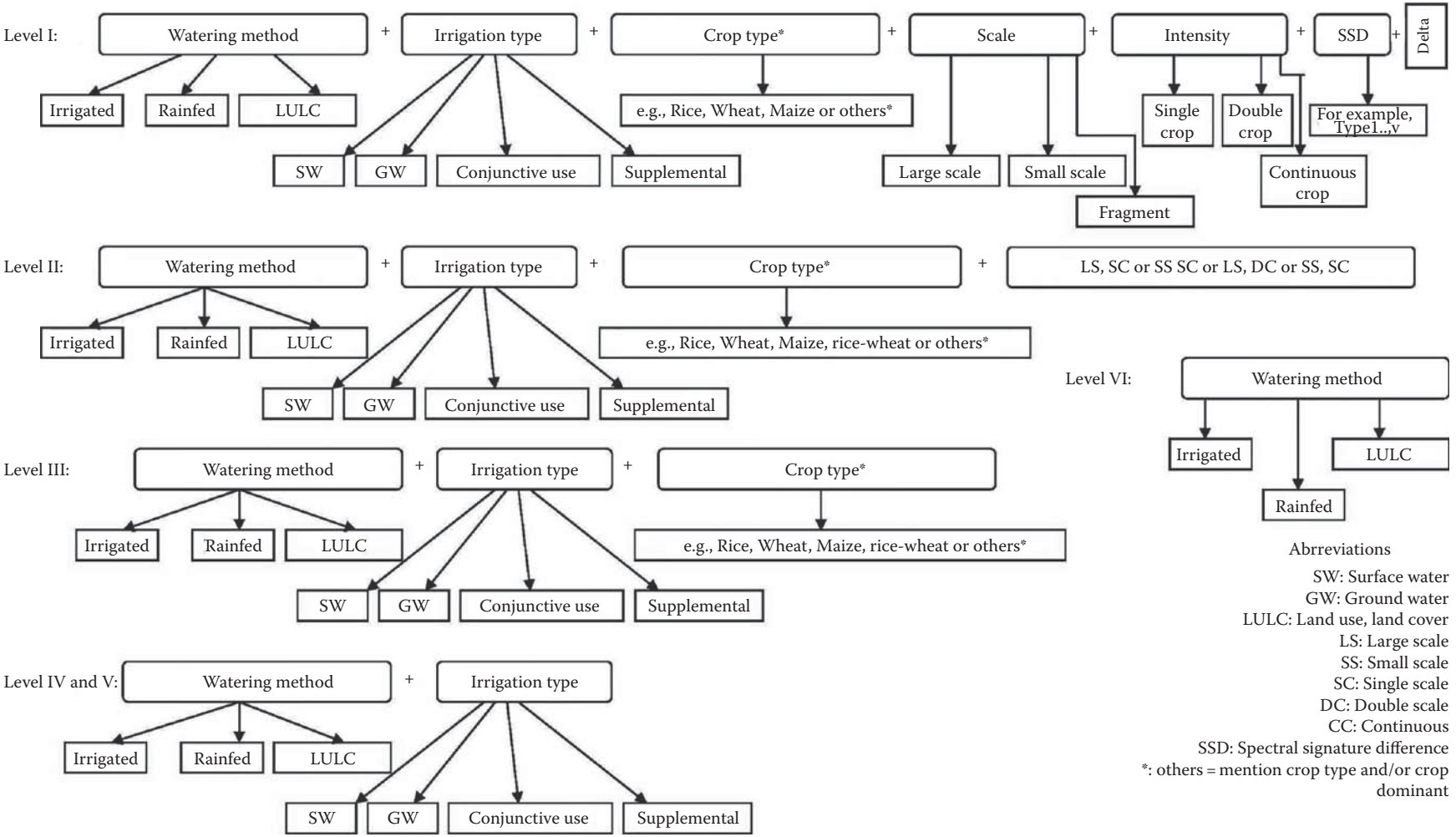

FIGURE 6.3 Cropland class naming convention at different levels. Level I is most detailed and Level IV is least detailed.

parameter would depend on many factors such as resolution of the imagery, available ground data, and expert knowledge. For example, if there is no sufficient knowledge on whether the irrigation is by surface water or ground water, but it is clear that the area is irrigated, one could just map it as irrigated without mapping greater details on the type of irrigation. But, for every cropland class, one has the potential to map the details as shown in Figure 6.3.

6.4 Definition of Remote Sensing–Based Cropland Mapping Products

Key to effective mapping is a precise and clear definition of what will be mapped. It is the first and primary step, with different definitions leading to different products. For example, irrigated areas are defined and understood differently in different applications and contexts. One can define them as areas that receive irrigation at least once during their crop growing period. Alternatively, they can be defined as areas that receive irrigation to meet at least half their crop water requirements during the growing season. One other definition can be that these are areas that are irrigated throughout the growing season. In each of these cases, the extent of irrigated area mapped will vary. Similarly, croplands can be defined as all agricultural areas irrespective of the types of crops grown or they may be limited to food crops (and not the fodder crops or plantation crops). So, it is obvious that having a clear understanding of the definitions of what we map is extremely important for the integrity of the products developed. We defined cropland products as follows:

- *Minimum mapping unit*: The minimum mapping unit of a particular crop is an area of 3 by 3 (0.81 ha) Landsat pixels identified as having the same crop type.
- *Cropland extent*: All cultivated plants harvested for food, feed, and fiber, *including* plantations (e.g., orchards, vineyards, coffee, tea, rubber).
- *What is a cropland pixel?: sub-pixel composition is used to calculate area. This involves multiplying full pixel area (FPA) with cropland area fraction (CAF). CAF provides what % of pixel is cropped. So, sub-pixel area/actual area = FPA*CAF*
- *Irrigated areas: Irrigation is defined as artificial application of any amount of water to overcome crop water stress. Irrigated areas are those areas that are irrigated one or more times during crop growing season.*
- *Rain-fed areas: Areas that have no irrigation whatsoever and are precipitation dependent.*
- *Cropping intensity: Number of cropping cycles within a 12-month period.*
- *Crop type: Eight crops (wheat, corn, rice, barley, soybeans, pulses, cotton, and potatoes), that occupy approx. 70% global cropland areas are considered. The rest of the crops are under "others". However, in particular continents where other crops like sugarcane or cassava etc. are important, they will be mapped as well.*

6.5 Data: Remote Sensing and Other Data for Global Cropland Mapping

Cropland mapping using remote sensing involves multiple types of data: satellite data with a consistent and useful global repeat cycle, secondary data, statistical data, and field plot data. When these data are used in an integrated fashion, the output products achieve highest possible accuracies (Thenkabail et al., 2009b,c).

6.5.1 Primary Satellite Sensor Data

Cropland mapping will require satellite sensor data across spatial, spectral, radiometric, and temporal resolutions from a wide array of satellite/sensor platforms (Table 6.2) throughout the growing season. These satellite sensors are "representative" of hyperspectral, multispectral, and hyperspatial data. The data points per hectare (Table 6.2, last column) will indicate the spatial detail of agricultural information gathered. In addition to satellite-based sensors, it is always valuable to gather ground-based hand-held spectroradiometer data from hyperspectral sensors (Thenkabail et al., 2013), and/or imaging spectroscopy from ground-based, airborne, or space borne sensors for validation and calibration purposes (Thenkabail et al., 2011). Much greater details of a wide array of sensors available to gather data are presented in Chapters 1 and 2 of *Remotely Sensed Data Characterization, Classification, and Accuracies*.

6.5.2 Secondary Data

There is a wide array of secondary or ancillary data such as the ASTER-derived digital elevation data (GDEM), long (50–100 years) records of precipitation and temperature (CRU), digital maps of soil types, and administrative boundaries. Many secondary data are known to improve crop classification accuracies (Thenkabail et al., 2009a,b). The secondary data will also form core data for the spatial decision support system and final visualization tool in many systems.

6.5.3 Field-Plot Data

Field-plot data (e.g., Figure 6.4) will be used for purposes such as: (1) class identification and labeling; (2) determining irrigated area fractions (AFs), and (3) establishing accuracies, errors, and uncertainties. At each field point (e.g., Figure 6.3), data such as cropland or noncropland, watering method (irrigated or rainfed), crop type, and cropping intensities are recorded along with GPS locations, digital photographs, and other information (e.g., yield, soil type) as needed. Field plot data will also help in gathering an ideal spectral data bank of croplands. One could use the precise locations and the crop characteristics and generate coincident remote sensing data characteristics (e.g., MODIS time-series monthly NDVI).

TABLE 6.2 Characteristics of Some of the Key Satellite Sensor Data Currently Used in Cropland Mapping

Satellite Sensor	Wavelength Range (μm)	Spatial Resolution (m)	Spectral Bands (#)	Temporal (days)	Radiometric (bits)	Data Points (per ha)
A. Hyperspectral						
EO-1 Hyperion			196	16	16	11.1 points for 30 m pixel
VNIR	0.43–0.93	30				(0.09 ha per pixel)
SWIR	0.93–2.40	30				
B. Advanced multispectral						
Landsat TM			7/8	16	8	
Multispectral						
Band 1	0.45–0.52	30				44.4 points for 15 m pixel
Band 2	0.53–0.61	30				11.1 points for 30 m pixel
Band 3	0.63–0.69	30				2.77 points for 60 m pixel
Band 4	0.78–0.90	30				0.69 points for 120 m pixel
Band 5	1.55–1.75	30				
Band 6	10.40–12.50	120/60				
Band 7	2.09–2.35	30				
Panchromatic	0.52–0.90	15				
EO-1 ALI			10	16	16	
Multispectral						
Band 1	0.43–0.45	30				
Band 2	0.45–0.52	30				
Band 3	0.52–0.61	30				
Band 4	0.63–0.69	30				
Band 5	0.78–0.81	30				
Band 6	0.85–0.89	30				
Band 7	1.20–1.30	30				
Band 8	1.55–1.75	30				
Band 9	2.08–2.35	30				
Panchromatic	0.48–0.69	10				
ASTER			14	16	8	
VNIR		15				
Band 1	0.52–0.60					
Band 2	0.63–0.69					
Band 3N/3B	0.76–0.86					
SWIR		30				
Band 4	1.600–1.700					
Band 5	2.145–2.185					
Band 6	2.185–2.225					
Band 7	2.235–2.285					
Band 8	2.295–2.365					
Band 9	2.360–2.430					
TIR		90				1.23 points for 90 m
Band 10	8.125–8.475					
Band 11	8.475–8.825					
Band 12	8.925–9.275					
Band 13	10.25–10.95					
Band 14	10.95–11.65					
MODIS						
MOD09Q1		250	2	1	12	0.16 points for 250 m
Band 1	0.62–0.67					
Band 2	0.84–0.876					

(*Continued*)

TABLE 6.2 (*Continued*) Characteristics of Some of the Key Satellite Sensor Data Currently Used in Cropland Mapping

Satellite Sensor	Wavelength Range (μm)	Spatial Resolution (m)	Spectral Bands (#)	Temporal (days)	Radiometric (bits)	Data Points (per ha)
MOD09A1		500	7[a]/36	1	12	0.04 points for 500 m
Band 1	0.62–0.67					
Band 2	0.84–0.876					
Band 3	0.459–0.479					
Band 4	0.545–0.565					
Band 5	1.23–1.25					
Band 6	1.63–1.65					
Band 7	2.11–2.16					
C. Hyperspatial						
GeoEye-1						
Multispectral		1.65	5	<3	11	
Band 1	0.45–0.52					59,488 points for 0.41 m
Band 2	0.52–0.60					26,874 points for 0.61 m
Band 3	0.63–0.70					10,000 points for 1 m
Band 4	0.76–0.90					3673 points for 1.65 m
Panchromatic	0.45–0.90	0.41				1679 points for 2.44 m
IKONOS			5	3	11	
Multispectral		4				
Band 1	0.45–0.52					625 points for 4 m
Band 2	0.51–0.60					400 points for 5 m
Band 3	0.63–0.70					236 points for 6.5 m
Band 4	0.76–0.85					100 points for 10 m
Panchromatic	0.53–0.93	1				44.4 points for 15 m
QuickBird			5	1–6	11	
Multispectral		2.44				
Band 1	0.45–0.52					
Band 2	0.52–0.60					
Band 3	0.63–0.69					
Band 4	0.76–0.90					
Panchromatic	0.45–0.90	0.61				
RapidEye		5–6.5	5	1–6	16	
Band 1	0.44–0.51					
Band 2	0.52–0.59					
Band 3	0.63–0.68					
Band 4	0.69–0.73					
Band 5	0.76–0.85					

[a] MODIS has 36 bands, but we considered only the first 7 bands (Mod09A1).

6.5.4 Very-High-Resolution Imagery Data

Very-high-resolution (submeter to 5 m) imagery (VHRI; see hyperspatial data characteristics in Table 6.2) is widely available these days from numerous sources. These data can be used as ground samples in localized areas to classify as well as verify classification results of the coarser resolution imagery. For example, in Figure 6.5, VHRI tiles identify uncertainties existing in cropland classification of coarser resolution imagery. VHRI is specifically useful for identifying croplands versus noncroplands (Figure 6.5). They can also be used for identifying irrigation based on associated features such as canals and tanks.

6.5.5 Data Composition: Mega File Data Cube (MFDC) Concept

Data preprocessing requires that all the acquired imagery is harmonized and standardized in known time intervals (e.g., monthly, biweekly). For this, the imagery data is either acquired or converted to at-sensor reflectance (see Chander et al., 2009; Thenkabail et al., 2004) and then converted to surface reflectance using Landsat Ecosystem Disturbance Adaptive Processing System (LEDAPS) codes for Landsat (Masek et al., 2006) or similar codes for other sensors. All data are processed and mosaicked to required geographic levels (e.g., global, continental). One method to organize these disparate but colocated datasets is through the

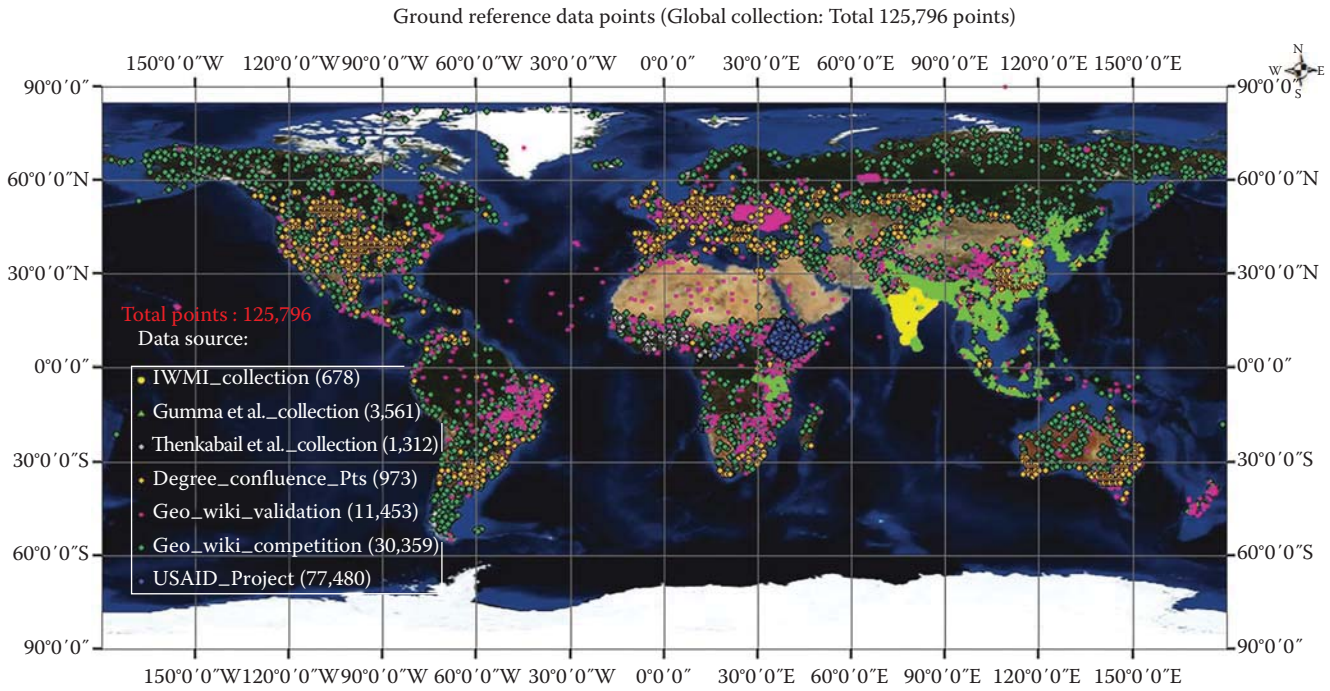

FIGURE 6.4 Field plot data for cropland studies collected over the globe.

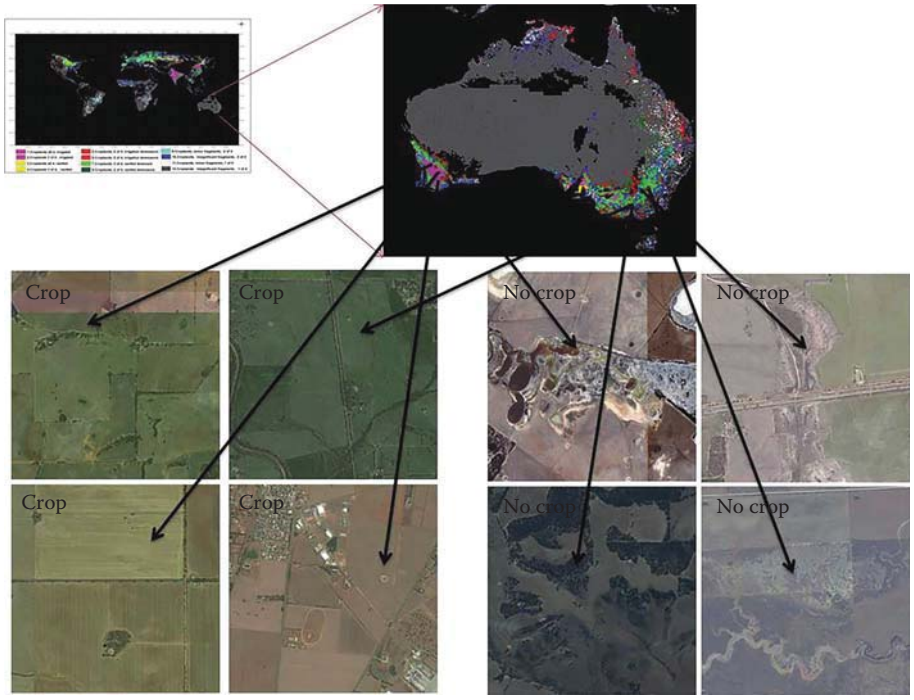

FIGURE 6.5 Very-high-resolution imagery used to resolve uncertainties in cropland mapping of Australia.

use of a MFDC. Numerous secondary datasets are combined in an MFDC, which is then stratified using image segmentation into distinct precipitation-elevation-temperature-vegetation zones. Data within the MFDC can include ASTER-derived refined digital elevation from SRTM (GDEM), monthly long-term precipitation, monthly thermal skin temperature, and forest cover and density. This segmentation allows cropland mapping to be focused; creating distinctive segments of MFDCs and analyzing them separately for croplands will enhance accuracy. For example, the likelihood of croplands in a temperature zone of <280°K is very low. Similarly, croplands in elevation above 1500 m will be of distinctive characteristics (e.g., patchy, on hilly terrain most likely plantations of coffee or tea). Every layer of data is geolinked (having precisely same projection and datum and are georeferenced to one another).

The purpose of MFDC (MFDC; see Thenkabail et al., 2009b for details) is to ensure numerous remote sensing and secondary data layers are all stacked one over the other to form a data cube akin to hyperspectral data cube. This approach has been used by X to map croplands in Y (reference). The MFDC allows us to have the entire data stack for any geographic location (global to local) as a single file available for analysis. For example, one can classify 10s or 100s or even 1000s of data layers (e.g., monthly MODIS NDVI time series data for a geographic area for an entire decade along with secondary data of the same area) stacked together in a single file and classify the image. The classes coming out of such a MFDC inform us about the phenology along with other characteristics of the crop.

6.6 Cropland Mapping Methods

6.6.1 Remote Sensing–Based Cropland Mapping Methods for Global, Regional, and Local Scales

There is a growing literature on cropland mapping across resolutions for both irrigated and rain-fed crops (Friedl et al., 2002; Gumma et al., 2011; Hansen et al., 2002; Kurz and Seelan, 2007; Loveland et al., 2000; Olofsson et al., 2011; Ozdogan and Woodcock, 2006; Thenkabail et al., 2009a,c; Wardlow and Egbert, 2008; Wardlow et al., 2006, 2007). Based on these studies, an ensemble of methods that is considered most efficient include: (1) spectral matching techniques (SMTs) (Thenkabail et al., 2007a, 2009a,c); (2) decision tree algorithms (DeFries et al., 1998); (3) Tassel cap brightness-greenness-wetness (Cohen and Goward, 2004; Crist and Cicone, 1984; Masek et al., 2008); (4) space-time spiral curves and change vector analysis (Thenkabail et al., 2005); (5) phenology (Loveland et al., 2000; Wardlow et al., 2006); and (6) climate data fusion with MODIS time-series spectral indices using decision tree algorithms and subpixel classification (Ozdogan and Gutman, 2008). More recently, cropland mapping algorithms that analyze end-member spectra have been used for global mapping by Thenkabail et al. (2009a, 2011).

6.6.2 Spectral Matching Techniques (SMTs) Algorithms

SMTs (Thenkabail et al., 2007a, 2009a, 2011) are innovative methods of identifying and labeling classes (see illustration in Figures 6.6 and 6.7a). For each derived class, this method identifies its characteristics over time using MODIS time-series data (e.g., Figure 6.6). NDVI time-series or other metrics (Biggs et al., 2006; Dheeravath et al., 2010; Thenkabail et al., 2005, 2007a) are analogous to spectra, where time is substituted for wavelength. The principle in SMT is to match the shape, or the magnitude or both to an ideal or target spectrum (pure class or "end-member"). The spectra at each pixel to be classified is compared to the end-member spectra and the fit is quantified using the following SMTs (Thenkabail et al., 2007a): (1) spectral correlation similarity (SCS)—a shape measure; (2) spectral similarity value (SSV)—a shape and magnitude measure; (3) Eucledian distance similarity (EDS)—a distance measure; and (4) modified spectral angle similarity (MSAS)—a hyperangle measure.

6.6.2.1 Generating Class Spectra

The MFDC (Section 6.4.5) of each of segment (Figures 6.6 and 6.7a) is processed using ISOCLASS K-means classification to produce a large number of class spectra with a unsupervised classification technique that are then interpreted and labeled. In more localized applications, it is common to undertake a field-plot data collection to identify and label class spectra. However, at the global scale, this is not possible due to the enormous resources required to cover vast areas to identify and label classes. Therefore, SMTs (Thenkabail et al., 2007a) to match similar classes or to match class spectra from the unsupervised classification with a library of ideal or target spectra (e.g., Figure 6.6a) will be used to identify and label the classes.

6.6.2.2 Creating Ideal Spectra Data Bank (ISDB)

The term "ideal or target" spectra refers to time-series spectral reflectivity or NDVI generated for classes for which we have precise location-specific ground knowledge. From these locations, signatures are extracted using MFDC, synthesized, and aggregated to generate a few hundred signatures that will constitute an ISDB (e.g., Figures 6.6 and 6.7a).

6.6.2.3 Matching Class Spectra with Ideal Spectra Using Spectral Matching Techniques (SMTs)

Once the class spectra are generated, they are compared with ideal spectra to match, identify, and label classes. Often quantitative spectral matching techniques like spectral correlation similarity R-square (SCS R-square) and spectral similarity value (SSV) are used (Thenkabail et al., 2007a).

6.7 Automated Cropland Classification Algorithm

The first part of the automated cropland classification algorithm (ACCA) method involves knowledge capture to understand and map agricultural cropland dynamics by: (1) identifying croplands versus noncroplands and crop type/dominance based on SMTs, decision trees tassel cap bispectral plots, and very-high-resolution imagery; (2) determining watering method (e.g., irrigated or rain-fed) based on temporal characteristics (e.g., NDVI), crop water requirement (water use by crops), secondary data (elevation, precipitation, temperature), and irrigation structure (e.g., canals and wells); (3) establishing croplands that are large scale (i.e., contiguous) versus small scale (i.e., fragmented); (4) characterizing cropping intensities (single, double, triple, and continuous cropping); (5) interpreting MODIS NDVI temporal bispectral plots to identify and label classes; and (6) using in situ data from very-high-resolution imagery, field-plot data, and national statistics (see Figure 6.7b for details). The second part of the method establishes accuracy of the knowledge-captured agricultural map (Congalton, 1991 and 2009) and statistics by comparison with national statistics, field-plot data, and very-high-resolution imagery. The third part of the method makes use of the captured knowledge to code and map cropland

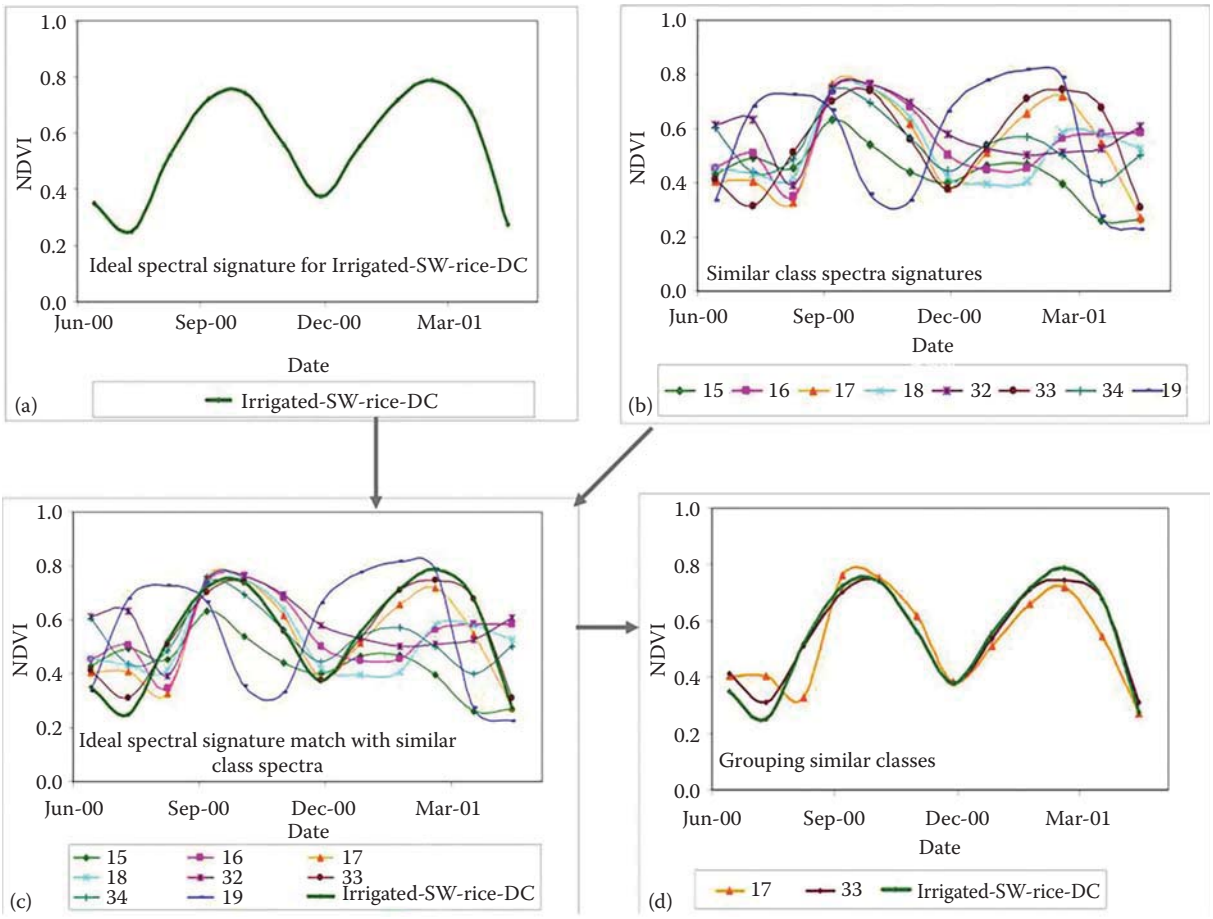

FIGURE 6.6 SMT. In SMTs, the class temporal profile (NDVI curves) are matched with the ideal temporal profile (quantitatively based on temporal profile similarity values) in order to group and identify classes as illustrated for a rice class in this figure. (a) Ideal temporal profile illustrated for "irrigated- surface-water-rice-double crop"; (b) some of the class temporal profile signatures that are similar; (c) ideal temporal profile signature (Figure 6.6a) matched with class temporal profiles (Figure 6.6b); and (d) the ideal temporal profile (Figure 6.6a, in deep green) matches with class temporal profiles of Classes 17 and 33 perfectly. Then one can label Classes 17 and 33 to be same as the ideal temporal profile ("irrigated-surface-water-rice-double crop"). This is a qualitative illustration of SMTs. For quantitative methods, refer to Thenkabail et al. (2007a).

dynamics through an automated algorithm. The fourth part of the method compares the agricultural cropland map derived using an automated algorithm (classified data) with that derived based on knowledge capture (reference map). The fifth part of the method applies the tested algorithm on an independent dataset of the same area to automatically classify and identify agricultural cropland classes. The sixth part of the method assesses accuracy and validates the classes derived from independent dataset using an automated algorithm (Thenkabail et al., 2012; Wu et al., 2014a,b).

6.8 Remote Sensing–Based Global Cropland Products: Current State-of-the-Art Maps, Their Strengths, and Limitations

Remote sensing offers the best opportunity to map and characterize global croplands most accurately, consistently, and repeatedly. Currently, there are three global cropland maps that have been developed using remote sensing techniques. In addition, we also considered a recent MODIS global land cover and land use map where croplands are included. We examined these maps to identify their strengths and weaknesses, to see how well they compare with each other, and to understand the knowledge gaps that need to be addressed. These maps were produced by:

1. Thenkabail et al. (2009b, 2011; Biradar et al., 2009)
2. Pittman et al. (2010)
3. Yu et al. (2013)
4. Friedl et al. (2010)

Thenkabail et al. (2009b, 2011; Figure 6.8; Table 6.3) used a combination of AVHRR, SPOT VGT, and numerous secondary (e.g., precipitation, temperature, and elevation) data to produce a global irrigated area map (Thenkabail et al., 2009b, 2011) and a global map of rain-fed cropland areas (Biradar et al., 2009; Thenkabail et al., 2011; Figure 6.8; Table 6.3). Pittman et al. (2010; Figure 6.9; Table 6.4) used MODIS 250 m data to map global cropland extent. More recently, Yu et al. (2013; Figure 6.10; Table 6.5) produced a

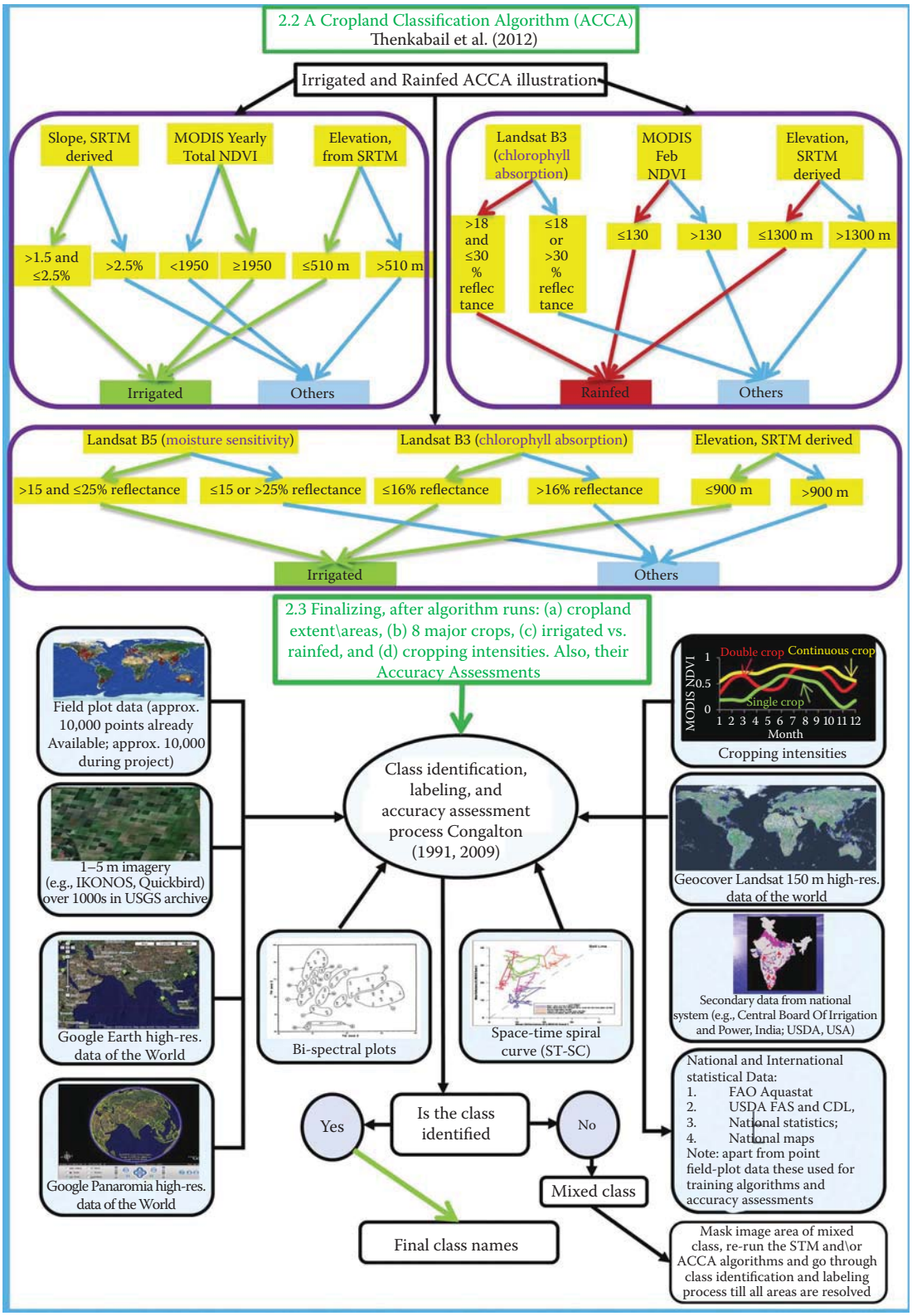

(a)

FIGURE 6.7 (a) Cropland mapping method illustrated here for a global scale (see Thenkabail et al., 2009b, 2011). The flowchart demonstrates comprehensive global cropland mapping methods using multisensor, multidate remote sensing, secondary, field plot, and very-high-resolution imagery data. (*Continued*)

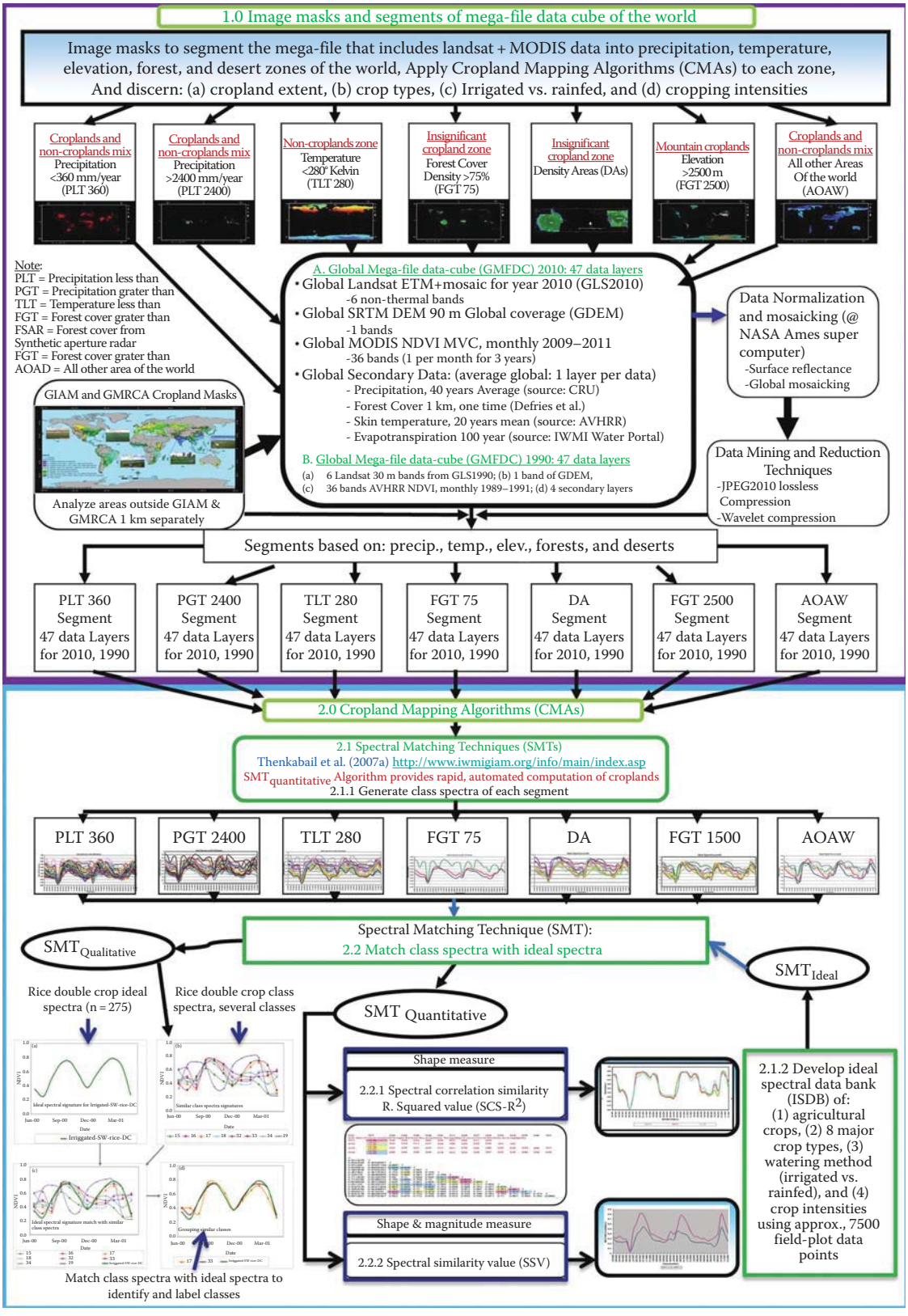

(b)

FIGURE 6.7 (*Continued*) (b) Cropland mapping methods illustrated for a global scale. Top half shows ACCA (see Thenkabail and Wu, 2012; Wu et al., 2014a) and bottom half shows class identification and labeling process.

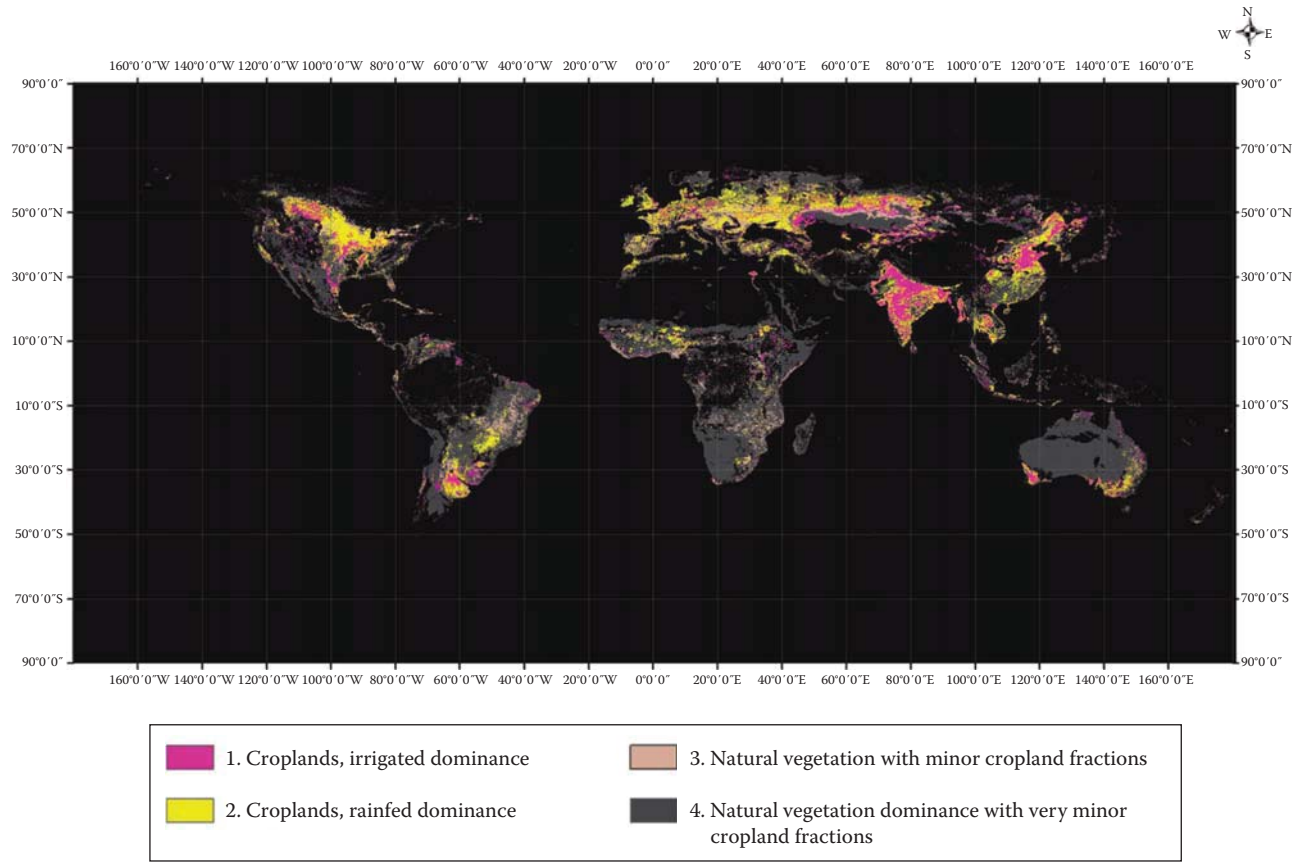

FIGURE 6.8 Global cropland product by Thenkabail et al. (2011, 2009b) using the method illustrated in Figure 6.7 and described in Section 6.1.1 (details in Thenkabail et al., 2011, 2009b). This includes irrigated and rain-fed areas of the world. The product is derived using remotely sensed data fusion (e.g., NOAA AVHRR, SPOT VGT, JERS SAR), secondary data (e.g., elevation, temperature, and precipitation), and in situ data. Total area of croplands is 2.3 billion hectares.

nominal 30 m resolution cropland extent of the world. These three global cropland extent maps are the best available current state-of-the-art products. Friedl et al. (2010; Figure 6.11; Table 6.6) used 500 m MODIS data in their global land cover and land use product (MCD12Q1) where croplands were one of the land cover classes. The methods, approaches, data, and definitions used in each of these products differ extensively. As a result, the cropland extents mapped by these products also vary significantly. The areas in Tables 6.3 through 6.6 only show the full pixel areas (FPAs) and not subpixel areas (SPAs). SPAs are actual areas, which can be estimated by reprojecting these maps to appropriate projections and calculating the areas. For the purpose of this chapter, we did not estimate SPAs. However, a comparison of the FPAs of the four maps (Figures 6.8 through 6.11) shows significant differences in the cropland areas (Tables 6.3 through 6.6) as well as significant differences in the precise locations of the croplands (Figures 6.8 through 6.11), the reasons for which are discussed in the next section.

TABLE 6.3 Global Cropland Extent at Nominal 1-km Based on Thenkabail et al. (2009b, 2011)[a]

Class #	Class Description (Names)	Pixels (1 km)	Percent (%)
1	Croplands, irrigated dominance	9,359,647	40
2	Croplands, rain-fed dominance	14,273,248	60
3	Natural vegetation with minor cropland fractions	5,504,037	
4	Natural vegetation dominance with very minor cropland fractions	44,170,083	
		23,632,895	100

[a] Total of approximately 2.3 billion hectares; Note that these are FPAs. Actual area is SPA. The SPA is not estimated here. See Thenkabail et al. (2007b) for the methods for calculating SPAs; % calculated based on Class 1 and 2. Class 3 and 4 are very small cropland fragments.

6.8.1 Global Cropland Extent at Nominal 1 km Resolution

We synthesized the four global cropland products discussed and produced a unified global cropland extent map GCE V1.0 at nominal 1 km (Table 6.7a; Figure 6.12a). The process involved resampling each global cropland product to a common resolution of 1 km and then performing GIS data overlays to determine where the cropland extents matched and where they differed.

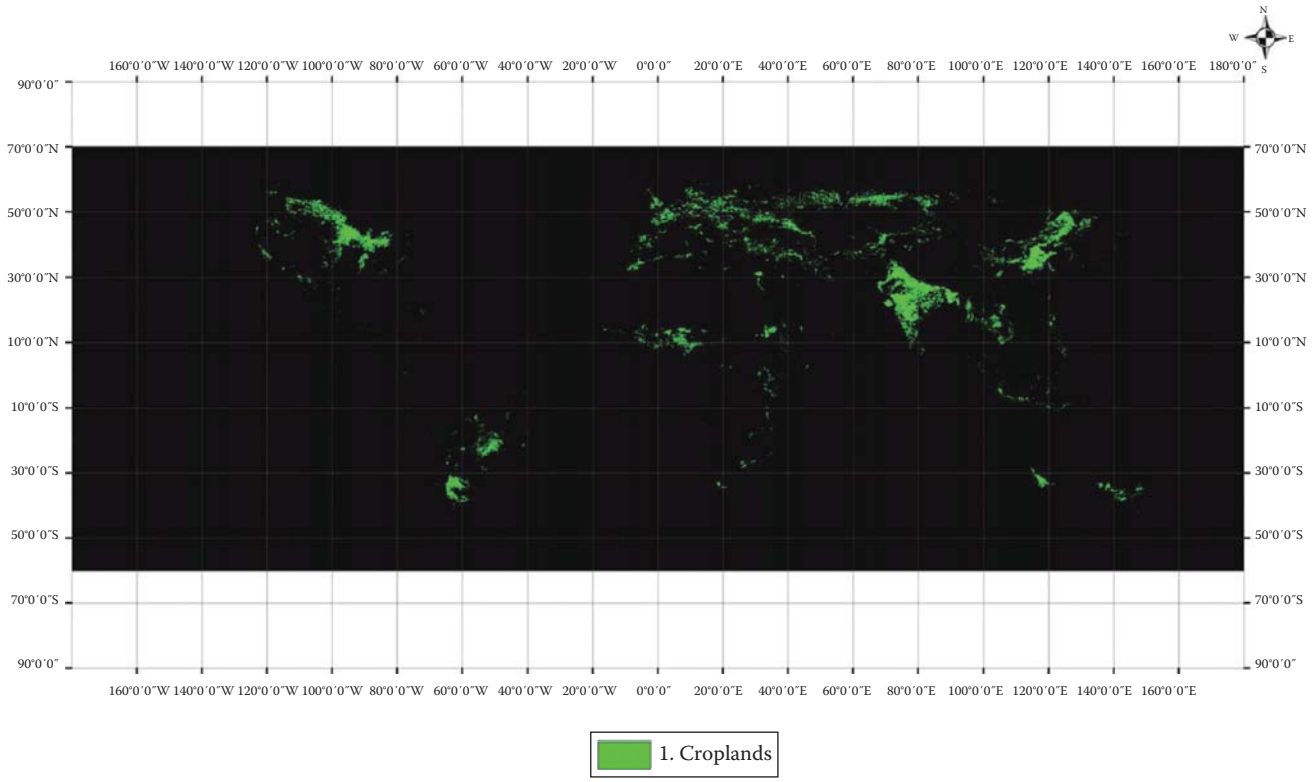

FIGURE 6.9 Global cropland extent map by Pittman et al. (2010) derived using MODIS 250 m data. There is only one cropland class, which includes irrigated and rain-fed areas of the world. There is no discrimination between rain-fed and irrigated areas. Total area of croplands is 0.9 billion hectares.

TABLE 6.4 Global Cropland Extent at Nominal 250 m Based on Pittman et al. (2010)[a]

Class #	Class Description (Names)	Pixels (1 km)	Percent (%)
1	Croplands	8,948,507	100

[a] Total of approximately 0.9 billion hectares. Note that these are FPAs. Actual area is SPA. SPA is not estimated here. See Thenkabail et al. (2007b) for the methods for calculating SPAs; % calculated based on Class 1.

Figure 6.12a shows the aggregated global cropland extent map with its statistics in Table 6.7a. Class 1 in Figure 6.12a and Table 6.7a provides the global cropland extent included in all four maps. Actual area of this extent is not calculated yet, but it includes approximately 2.3 billion hectares FPAs (Table 6.7a). The spatial distribution of these 2.3 billion hectares is demonstrated as Class 1 in Figure 12a. Classes 2 and 3 are areas with minor or very minor cropland fractions. Class 2 and Class 3 are classes with large areas of natural vegetation and/or desert lands and other lands.

Figure 6.12b and Table 6.7b demonstrate where and by how much the four products match with one another. For example, 2,802,397 pixels (Class 1, Table 6.7b; Figure 6.12b) are croplands that are irrigated. Some of the products do not separately classify irrigated versus rain-fed croplands, although all four products show where croplands are. We first identified where all four products match as croplands and then added irrigation status or other indicators (e.g., irrigation dominance, rain-fed; Table 6.7b) from the product by Thenkabail et al. (2009b, 2011).

Table 6.7b and Figure 6.12b show 12 classes of which Classes 1 and 2 are croplands with irrigated agriculture, Classes 3 and 4 are croplands with rain-fed agriculture, Classes 5 and 6 are croplands where irrigated agriculture dominates, Classes 7 and 8 are croplands where rain-fed agriculture dominates, and Classes 9–12 are areas with minor or very minor cropland fractions. Classes 9–12 are those with large areas of natural vegetation and\or desert lands and other lands.

Interestingly, and surprisingly as well, only 20% (Class 1 and 3; Table 6.7b; Figure 6.12b) of the total cropland extent are matched precisely in all four products. Further, 49% (Class 1, 2, 3, 4, and 7; Table 6.7b; Figure 6.12b) of the total cropland areas match in at least three of the four products. This implies that all the four products have considerable uncertainties in determining the precise location of the croplands. The great degree of uncertainty in the cropland products can be attributed to factors including

1. Coarse resolution of the imagery used in the study
2. Definition of mapping products of interest
3. Methods and approaches adopted
4. Limitations of the data

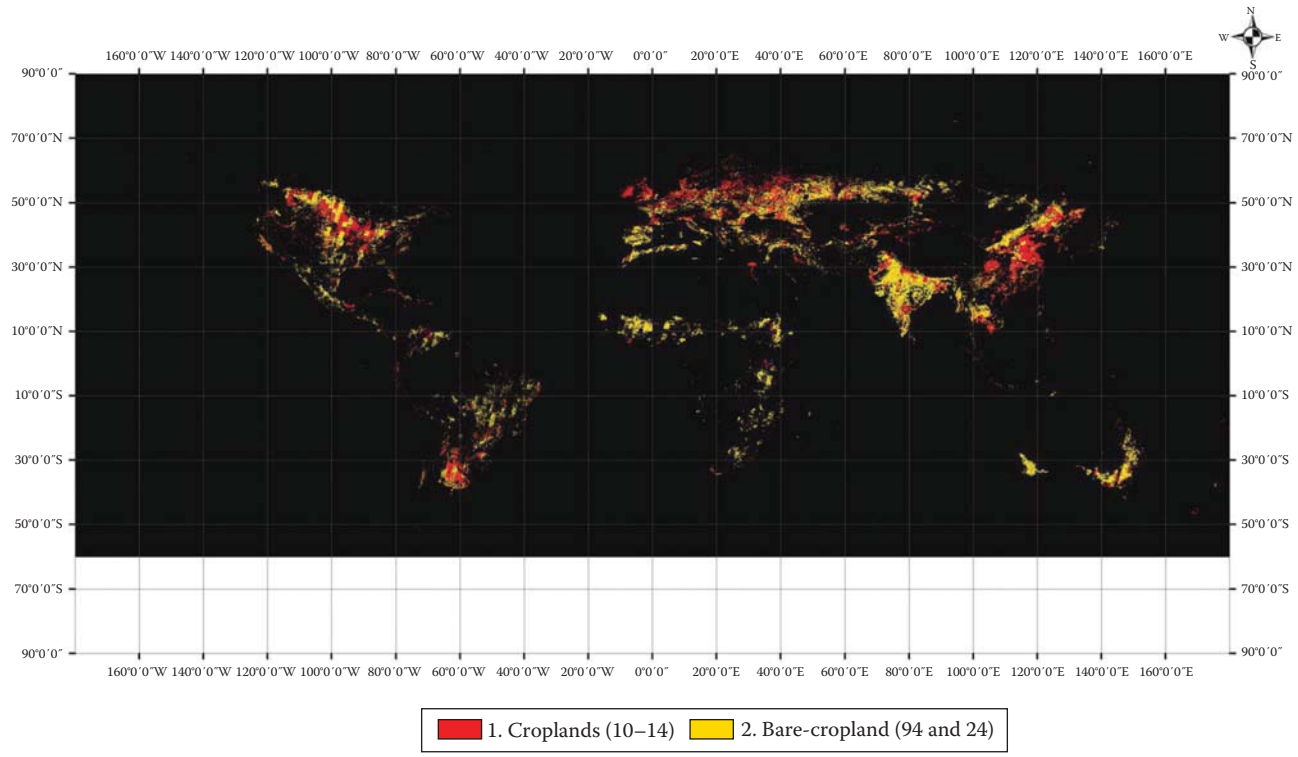

FIGURE 6.10 Global cropland extent map by Yu et al. (2013) derived at nominal 30 m data. Total area of croplands is 2.2 billion hectares. There is no discrimination between rain-fed and irrigated areas.

TABLE 6.5 Global Cropland Extent at Nominal 30 m Based on Yu et al. (2013)[a]

Class #	Class Description (Names)	Pixels (1 km)	Percent
1	Croplands (Classes 10–14)	7,750,467	35
2	Bare-cropland (Classes 94 and 24)	14,531,323	65
		22,281,790	100

[a] Total of approximately 2.2 billion hectares. Note that these are FPAs. Actual area is SPA. SPA is not estimated here. See Thenkabail et al. (2007b) for the methods for calculating SPAs; % calculated based on Class 1 and 2.

Table 6.7c and Figure 6.12c show five classes of which Classes 1 and 2 are croplands with irrigated agriculture, Class 3 is cropland with rain-fed agriculture, Classes 4 and 5 have ONLY minor or very minor cropland fractions. We recommend the use of this aggregated five class global cropland map (Figure 12c and Table 6.7c) produced based on the four major cropland mapping efforts [i.e., Thenkabail et al. (2009a, 2011), Pittman et al. (2010), Yu et al. (2013), and Friedl et al. (2010)] using remote sensing. This map (Figure 6.12c; Table 6.7c) provides clear consensus view on of four major studies on global:

- Cropland extent location
- Cropland watering method (irrigation versus rain-fed)

The product (Figure 6.12c; Table 6.7c) does not show where the crop types are or even the crop dominance. However, cropping intensity can be gathered using multitemporal remote sensing over these cropland areas.

6.9 Change Analysis

Once the croplands are mapped (Figure 6.13), we can use the time-series historical data such as continuous global coverage of remote sensing data from NOAA very-high-resolution radiometer (VHRR) and advanced VHRR (AVHRR), Global Inventory Modeling and Mapping Studies (GIMMS; 1982–2000), and MODIS time-series (2001–present) to help build an inventory of historical agricultural development (e.g., Figures 6.13 and 6.14). Such an inventory will provide information including identifying areas that have switched from rain-fed to irrigated production (full or supplemental), and noncropped to cropped (and vice versa). A complete history will require systematic analysis of remotely sensed data as well as a systematic compilation of all routinely populated cropland databases from the agricultural departments of all countries throughout the world. The differences in pixel sizes in AVHRR versus MODIS will: (1) influence class

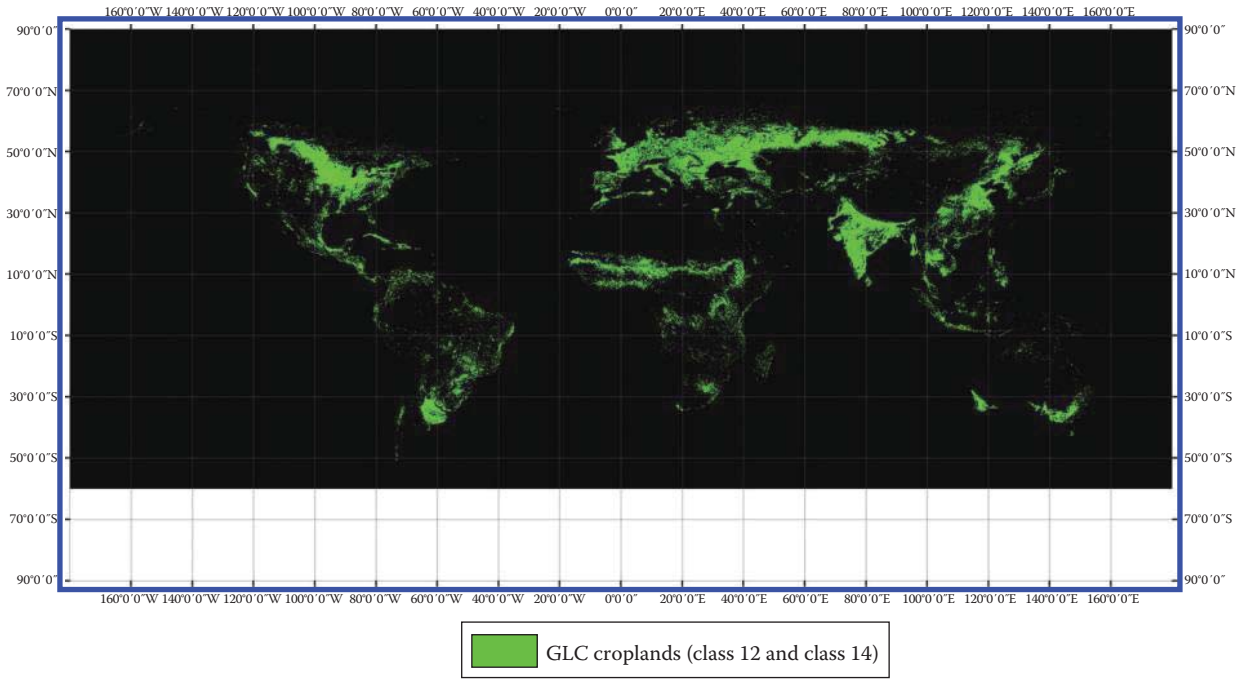

FIGURE 6.11 Global cropland classes (Class 12 and Class 14) extracted from MODIS Global land use and land cover (GLC) 500 m product MCD12Q2 by Friedl et al. (2010). Total area of croplands is 2.7 billion hectares. There is no discrimination between rain-fed and irrigated cropland areas.

TABLE 6.6 Global Cropland Extent at Nominal 500 m Based on Friedl et al. (2010)[1]

Class #	Class Description (Names)	Pixels (1 km)	Percent
1	Global croplands (Class 12 and 14)	27,046,084	100

[a] Approximately, total 2.7 billion hectares based on Class 12 and 14. Note that these are FPAs. Actual area is SPA. SPA is not estimated here. See Thenkabail et al. (2007b) for the methods for calculating SPAs.

identification and labeling, and (2) cause different levels of uncertainties. We will address these issues by determining SPAs and uncertainties involved in class accuracies and uncertainties in areas at various spatial resolutions using methods detailed in recent work of this team (Ozdogan and Woodcock, 2006; Thenkabail et al., 2007b; Velpuri et al., 2009). Change analyses (Tomlinson, 2003) are conducted in order to investigate both the spatial and temporal changes in croplands (e.g., Figures 6.13 and 6.14) that will help establish: (1) change in total cropland areas, (2) change in spatial location of cropland areas, (3) expansion on croplands into natural vegetation, (4) expansion of irrigation, (5) change from croplands to biofuels, and (6) change from croplands to urban. Massive reductions in cropland areas in certain parts of the world will be detected, including cropland lost as a result of reductions in available ground water supply due to overdraft (Jiang, 2009; Rodell et al., 2009; Wada et al., 2012).

6.10 Uncertainties of Existing Cropland Products

Currently, the main causes of uncertainties in areas reported in various studies (Ramankutty et al., 2008; Thenkabail et al., 2009a,c) can be attributed to, but not limited to: (1) reluctance of national and state agencies to furnish the census data on irrigated area and concerns of their institutional interests in sharing of water and water data; (2) reporting of large volumes of census data with inadequate statistical analysis; (3) subjectivity involved in the observation-based data collection process; (4) inadequate accounting of irrigated areas, especially minor irrigation from groundwater, in national statistics; (5) definitional issues involved in mapping using remote sensing as well as national statistics; (6) difficulties in arriving at precise estimates of AFs using remote sensing; (7) difficulties in separating irrigated from rain-fed croplands; and (8) imagery resolution in remote sensing. Other limitations include (Thenkabail et al., 2009a, 2011)

1. Absence of precise spatial location of the cropland areas for training and validation
2. Uncertainties in differentiating irrigated areas from rain-fed areas
3. Absence of crop types and cropping intensities
4. Inability to generate cropland maps and statistics, routinely
5. Absence of dedicated web\data portal for dissemination cropland products

TABLE 6.7 Global Cropland Extent at Nominal 1-km Based on Four Major Studies: Thenkabail et al. (2009b, 2011), Pittman et al. (2010), Yu et al. (2013), and Friedl et al. (2010).

Class #	Class Description (Names)	Pixels (1 km)	Percent (%)
(a) *Three class map*[a]			
1	Croplands	23,493,936	100
2	Cropland minor fractions	13,700,176	
3	Cropland very minor fractions	44,662,570	
(b) *Twelve class map*[b]			
1	Croplands all 4, irrigated	2,802,397	12
2	Croplands 3 of 4, irrigated	289,591	1
3	Croplands all 4, rain-fed	1,942,333	8
4	Croplands 3 of 4, rain-fed	427,731	2
5	Croplands, 2 of 4, irrigation dominance	3,220,330	14
6	Croplands, 2 of 4, irrigation dominance	1,590,539	7
7	Croplands, 3 of 4, rain-fed dominance	6,206,419	26
8	Croplands, 2 of 4, rain-fed dominance	3,156,561	13
9	Croplands, minor fragments, 2 of 4	3,858,035	17
10	Croplands, very minor fragments, 2 of 4	6,825,290	
11	Croplands, minor fragments, 1 of 4	6,874,886	
12	Croplands, very minor fragments, 1 of 4	44,662,570	
	Class 1–9 total	23,493,936	100
(c) *Five class map*[c]			
1	Croplands, irrigation major	3,091,988	13
2	Croplands, irrigation minor	4,810,869	21
3	Croplands, rain-fed	11,733,044	50
4	Croplands, rain-fed minor fragments	3,858,035	16
5	Croplands, rain-fed very minor fragments	13,700,176	
	Classes 1–4 total	23,493,936	100.0%

[a] Approximately 2.3 billion hectares (Class 1) of cropland is estimated. But this is full pixel area (FPA). Actual area is sub pixel area (SPA). SPA is not estimated here. See Thenkabail et al. (2007b) for the methods for calculating SPAs; % calculated based on Class 1; Class 2 and 3 are minor/very minor cropland fragments.

[b] Approximately 2.3 billion hectares (Class 1–9) of cropland is estimated. But this is FPA. Actual area is SPA. SPA is not estimated here. See Thenkabail et al. (2007b) for the methods for calculating SPAs; % calculated based on Class 1–9; Classes 10, 11, and 12 are minor cropland fragments; All 4 means, all 4 studies agreed.

[c] Approximately 2.3 billion hectares (Class 1–4) of cropland is estimated. But this is FPA. Actual area is SPA. SPA is not estimated here. See Thenkabail et al. (2007b) for the methods for calculating SPAs; % calculated based on Class 1–4; Class 5 is very minor cropland fragments.

These limitations are a major hindrance in accurate/reliable global, regional, and country-by-country water use assessments that in turn support crop productivity (productivity per unit of land, kg/m^2) studies, water productivity (productivity per unit of water, kg/m^3) studies, and food security analyses. The higher degrees of uncertainty in coarser resolution data are a result of an inability to capture fragmented, smaller patches of croplands accurately, and the homogenization of both crop and noncrop land within areas of patchy land cover distribution. In either case, there is a strong need for finer spatial resolution to resolve the confusion.

6.11 Way Forward

Given the aforementioned issues with existing maps of global croplands, the way forward will be to produce global cropland maps at finer spatial resolution and applying a suite of advanced analysis methods. Previous research has shown that at finer spatial resolution, the accuracy of irrigated and rain-fed area class delineations improves, because at finer spatial resolution, more fragmented and smaller patches of irrigated and rain-fed croplands can be delineated (Ozdogan and Woodcock, 2006; Velpuri et al., 2009). Further, greater details of crop characteristics such as crop types (e.g., Figure 6.15) can be determined at finer spatial resolutions. Crop type mapping will involve the use of advanced methods of analysis such as data fusion of higher spatial resolution images from sensors such as Resourcesat\Landsat and AWiFS\MODIS (e.g., Table 6.2) supported by extensive ground surveys and ideal spectral data bank (ISDB) (Thenkabail et al., 2007a). Harmonic analysis is often adopted to identify crop types (Sakamoto et al., 2005) using methods such as the conventional Fourier analysis and adopting a Fourier filtered cycle similarity (FFCS) method. Mixed classes are resolved using hierarchical crop mapping

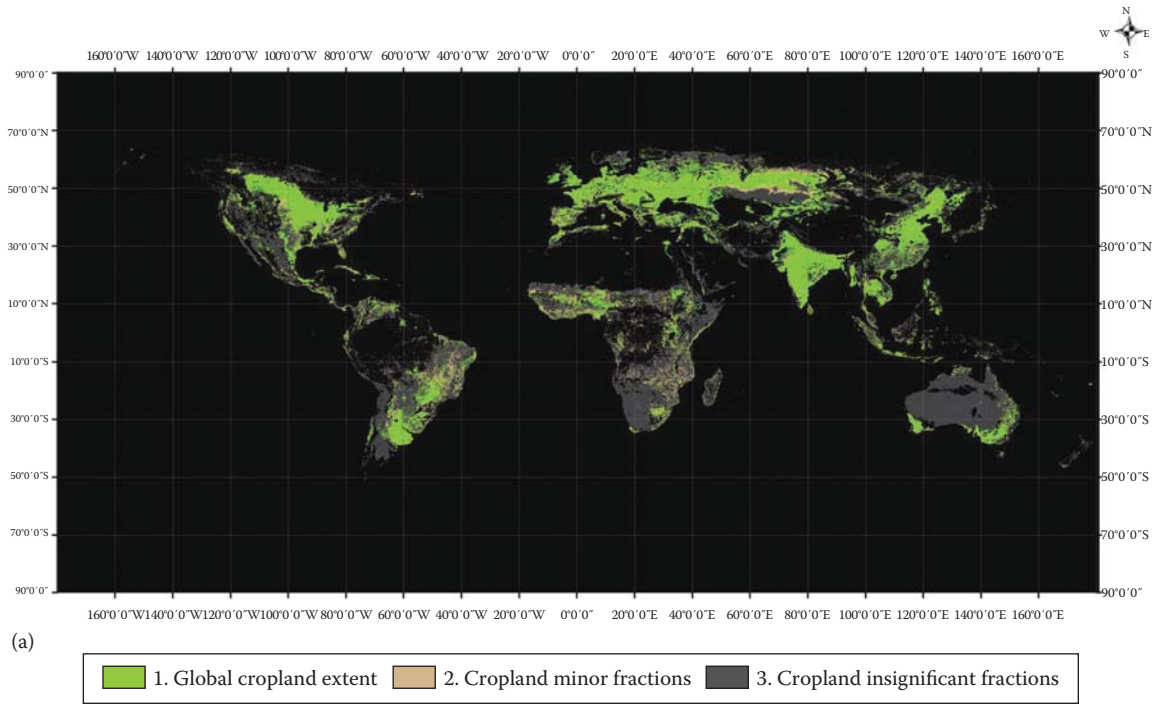

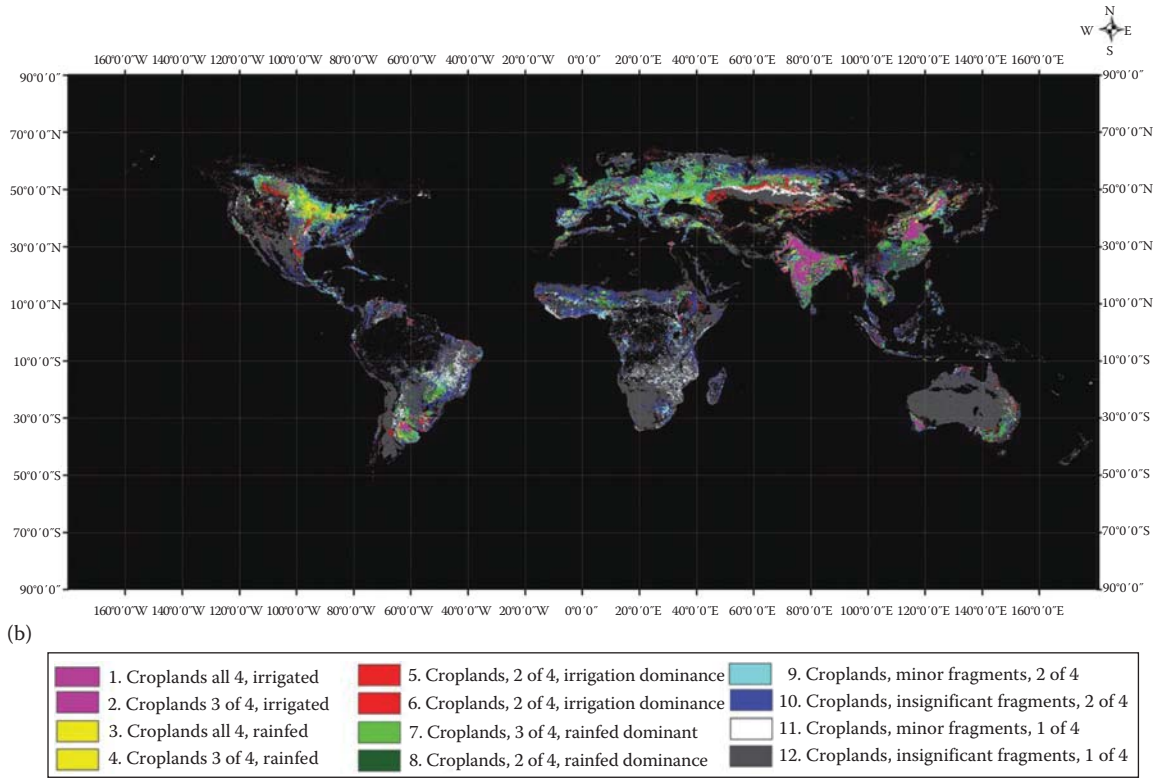

FIGURE 6.12 (a) An aggregated three class global cropland extent map at nominal 1 km based on four major studies: Thenkabail et al. (2009a, 2011), Pittman et al. (2010), Yu et al. (2013), and Friedl et al. (2010). Class 1 is total cropland extent; total cropland extent is 2.3 billion hectares (FPAs). Class 2 and Class 3 have ONLY minor fractions of croplands. Refer to Table 6.7a for cropland statistics of this map. (b) A disaggregated twelve class global cropland extent map derived at nominal 1-km based on four major studies: Thenkabail et al. (2009a, 2011), Pittman et al. (2010), Yu et al. (2013), and Friedl et al. (2010). Classes 1–9 are cropland classes that are dominated by irrigated and rain-fed agriculture. Classes 10–12 have ONLY minor or very minor fractions of croplands. Refer to Table 6.7b for cropland statistics of this map. (*Continued*)

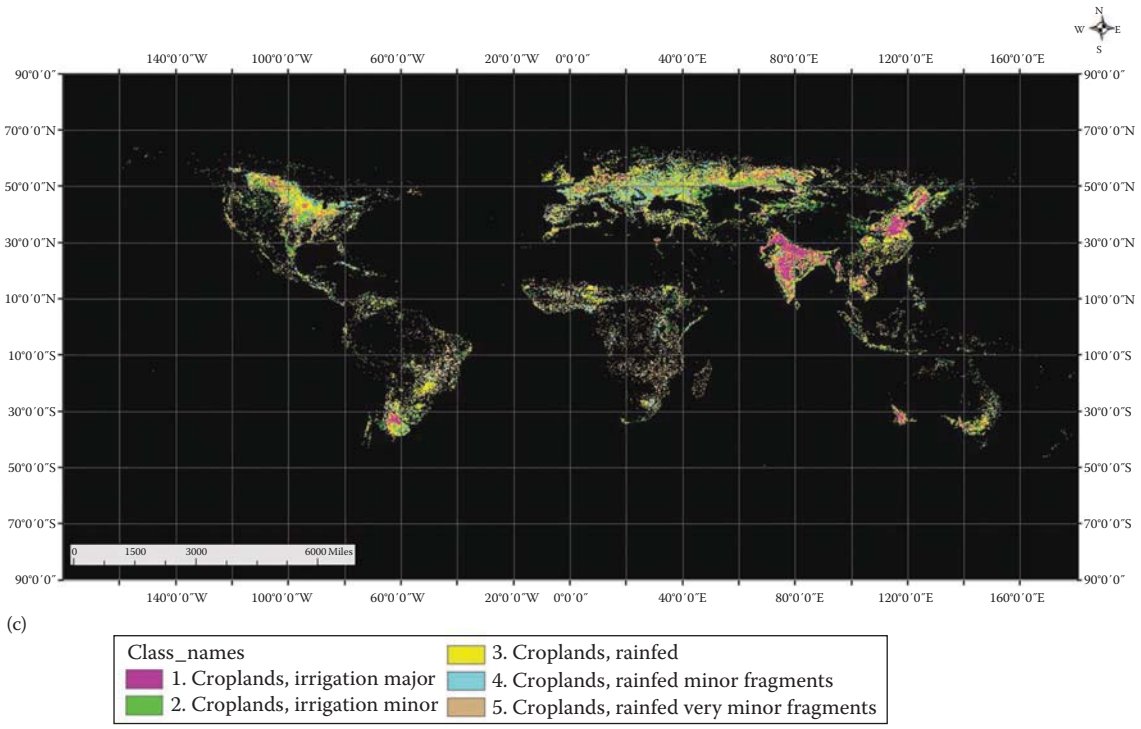

FIGURE 6.12 (*Continued*) (c) A disaggregated five class global cropland extent map derived at nominal 1-km based on four major studies: Thenkabail et al. (2009a, 2011), Pittman et al. (2010), Yu et al. (2013), and Friedl et al. (2010). Classes 1–5 are cropland classes, that are dominated by irrigated and rain-fed agriculture. However, Class 4 and Class 5 have ONLY minor or very minor fractions of croplands. Refer to Table 6.7c for cropland statistics of this map. Note: *Irrigation major*: areas irrigated by large reservoirs created by large and medium dams, barrages, and even large ground water pumping. *Irrigation minor*: areas irrigated by small reservoirs, irrigation tanks, open wells, and other minor irrigation. However, it is very hard to draw a strict boundary between major and minor irrigations and in places, there can be significant mixing. Major irrigated areas such as the Ganges basin, California's central valley, Nile basin, etc., are clearly distinguishable as major irrigation, and in other areas major and minor irrigation may be intermixed.

protocol based on decision tree algorithm (Wardlow and Egbert, 2008). Irrigated versus rain-fed croplands will be distinguished using spectral libraries (Thenkabail et al., 2007b) and ideal spectral data banks (Thenkabail et al., 2007a, 2009a). Similar classes will be grouped by matching class spectra with ideal spectra based on SMTs (SMTs; Thenkabail et al., 2007a). Details such as crop types are crucial for determining crop water use, crop productivity, and water productivity, leading to providing crucial information needed for food security studies. However, the high spatial resolution must be fused with high temporal resolution data in order to obtain time-series spectra that are crucial for monitoring crop growth dynamics and cropping intensity (e.g., single crop, double crop, and continuous year round crop). Numerous other methods and approaches exist. But, the ultimate goal using multisensor remote sensing is to produce croplands products such as

1. Cropland extent\area
2. Crop types (initially focused on eight crops that occupy 70% of global croplands)
3. Irrigated versus rain-fed croplands
4. Cropping intensities\phenology (single, double, triple, and continuous cropping)
5. Cropped area computation
6. Cropland change over space and time

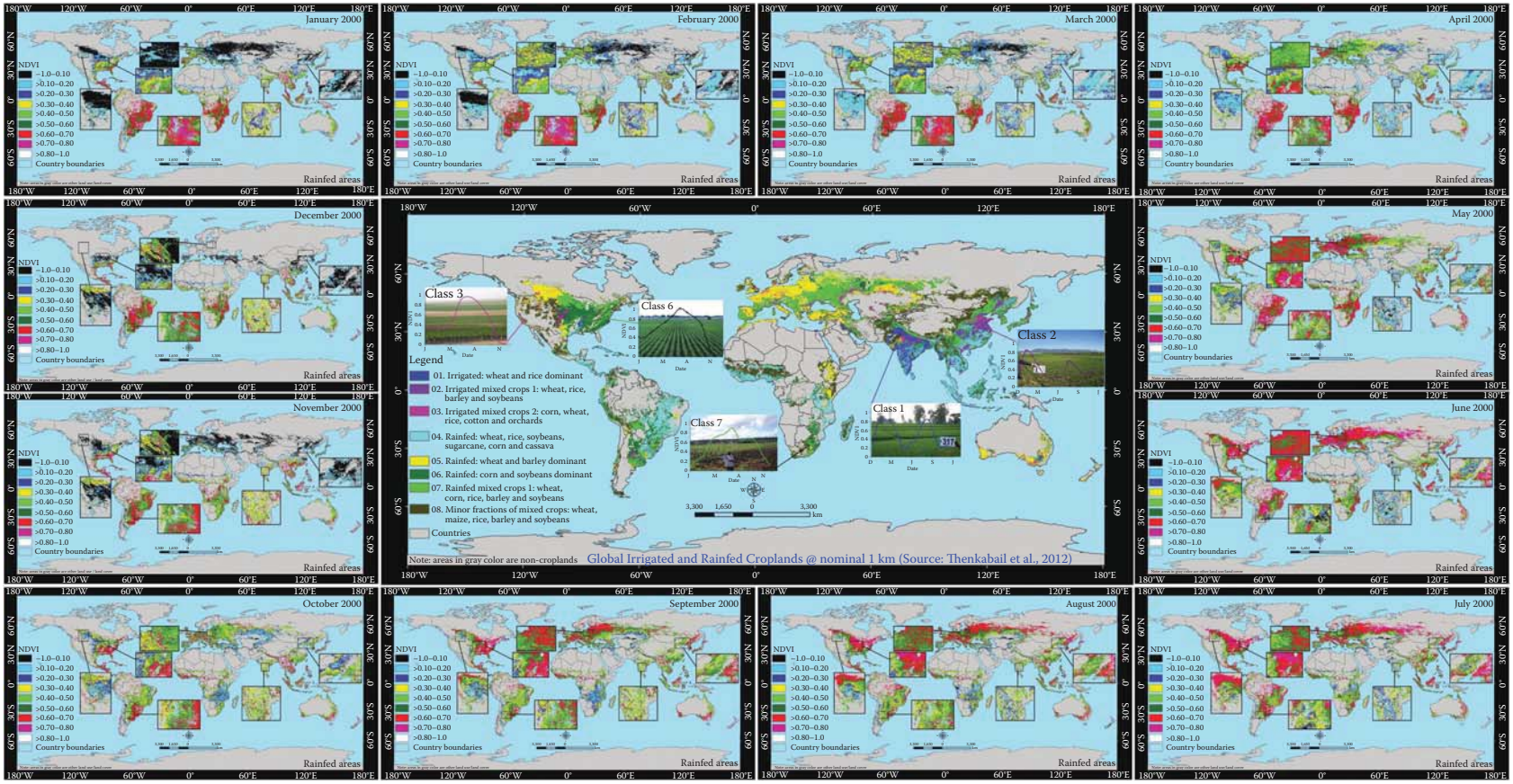

FIGURE 6.13 Center image of global cropland (irrigated and rainfed) areas @ 1 km for year 2000 produced by overlying the remote sensing derived product of the International Water Management Institute (IWMI; Thenkabail et al., 2012, 2011, 2009a,b; http://www.iwmigiam.org) over five dominant crops (wheat, rice, maize, barley, and soybeans) of the world produced by Ramankutty et al. (2008). The five crops constitute about 60% of all global cropland areas. The IWMI remote sensing product is derived using remotely sensed data fusion (e.g., NOAA AVHRR, SPOT VGT, and JERS SAR), secondary data (e.g., elevation, temperature, and precipitation), and *in situ* data. Total area of croplands is 1.53 billion hectares, of which 399 million hectares is total area available for irrigation (without considering cropping intensity) and 467 million hectares is annualized irrigated areas (considering cropping intensity). Surrounding NDVI images of irrigated areas: From January to December irrigated area NDVI dynamics is produced using NOAA AVHRR NDVI. The irrigated areas were determined by Thenkabail et al. (2011, 2009a,b).

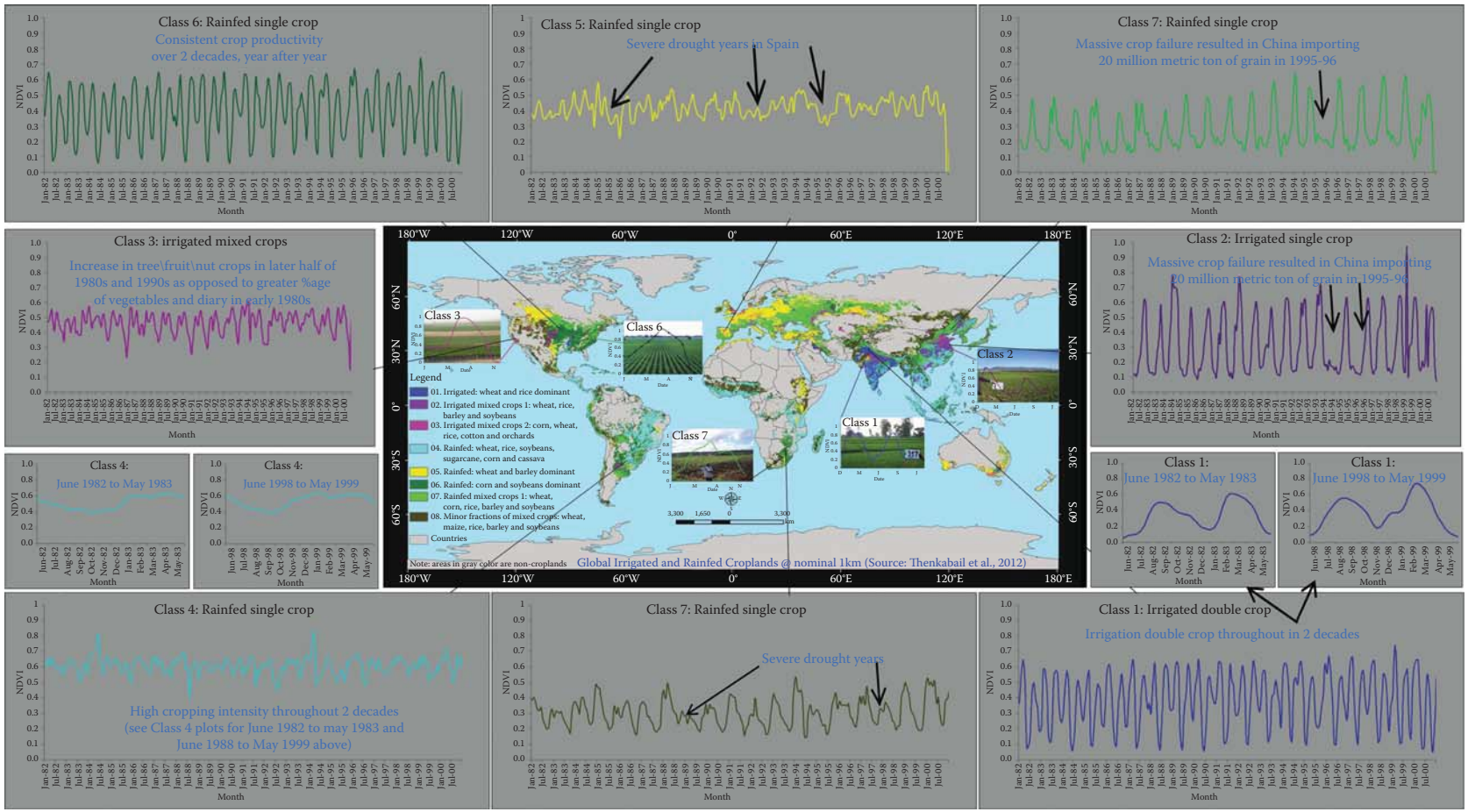

FIGURE 6.14 Global agricultural dynamics over two decades illustrated here for some of the most significant agricultural areas of the World. Once we establish GCAD2010 and GCAD1990 at nominal 30 m resolution for the entire world, we will use AVHRR-MODIS monthly MVC NDVI time-series from 1982 to 2017 to provide a continuous time history of global irrigated and rain-fed croplands, establish their spatial and temporal changes, and highlight the hot spots of change. The GCAD2010, GCAD1990, and GCAD four decade's data will be made available on USGS global cropland data portal (currently under construction): http://powellcenter.usgs.gov/current_projects.php#GlobalCroplandsAbstract. Further, the need to map accurately specific cropland characteristics such as crop types and watering methods (e.g., irrigated versus rain-fed) is crucial in food security analysis. For example, the importance of irrigation to global food security is highlighted in a recent study by Siebert and Döll (2010) who show that without irrigation, there would be a decrease in production of various foods including dates (60%), rice (39%), cotton (38%), citrus (32%), and sugarcane (31%) from their current levels. Globally, without irrigation, cereal production would decrease by a massive 43%, with overall cereal production, from irrigated and rain-fed croplands, decreasing by 20%.

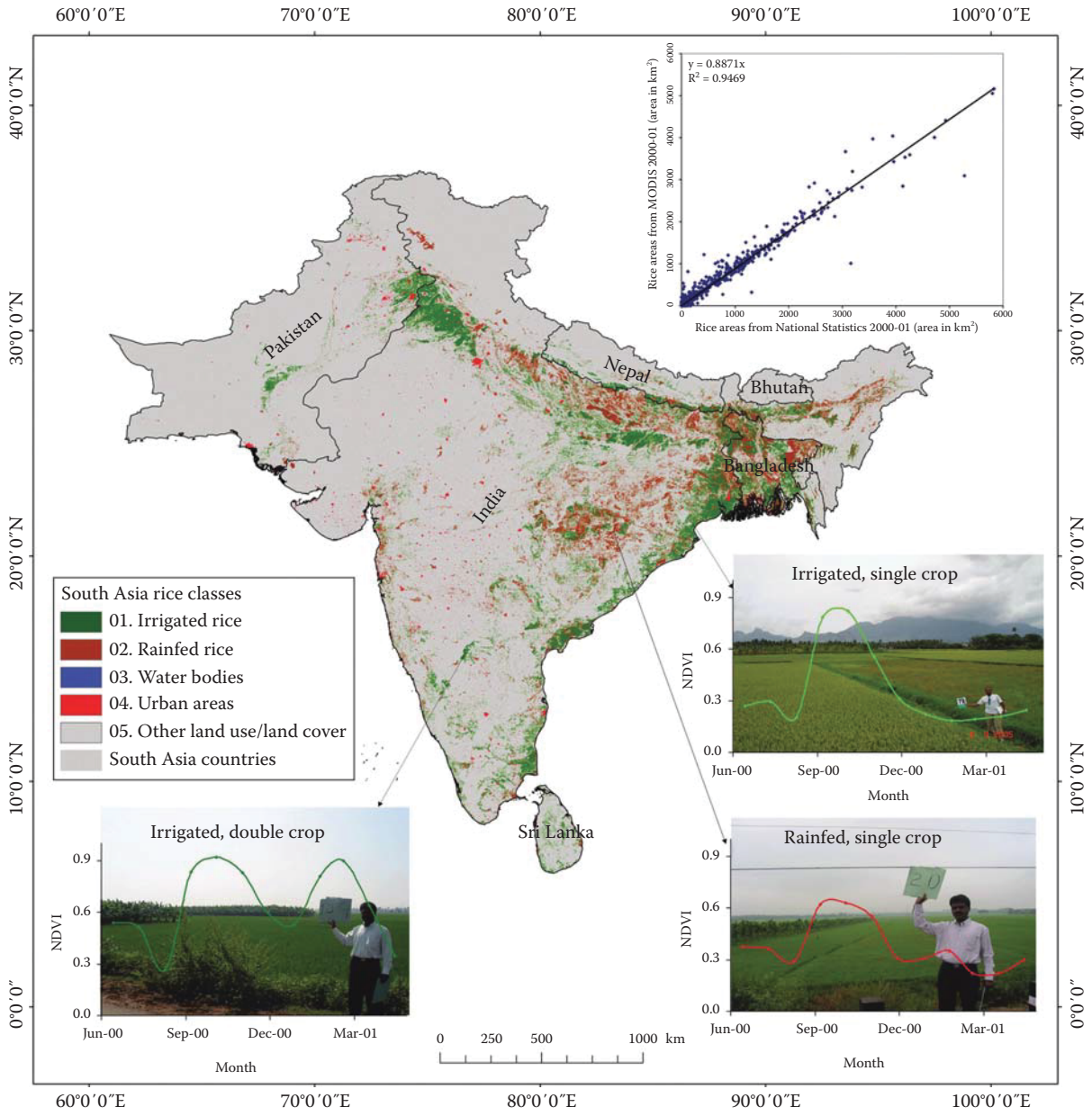

FIGURE 6.15 Rice map of south Asia produced using the method illustrated in Figure 6.6. (From Gumma, M. K. et al., *J. Appl. Rem. Sens.*, 5, 053547, September 1, 2011, doi:10.1117/1.3619838, 2011.)

6.12 Conclusions

This chapter provides an overview of the importance of global cropland products in food security analysis. It is obvious that only remote sensing from Earth-observing (EO) satellites provides consistent, repeated, high-quality data for characterizing and mapping key cropland parameters for global food security analysis. Importance of definitions and class naming conventions in cropland mapping has been reiterated. Typical EO systems and their spectral, spatial, temporal, and radiometric characteristics useful for cropland mapping have been highlighted. The chapter provides a review of various cropland mapping methods used at global, regional, and local levels. Some of the remote sensing methods for global cropland mapping have been illustrated. The current state-of-the-art provides four-key global cropland products (-e.g., Figure 6.12) derived from remote sensing, based on the work conducted by four major studies (Thenkabail et al. (2009a, 2011, Pittman et al. 2010, Yu et al. 2013, and Friedl et al. 2010). These studies were conducted using: (1) time-series of multisensor data and secondary data, (2) 250 m MODIS time-series data, (3) 30 m Landsat data, and (4) a MODIS 500 m time-series derived cropland classes from a land use\land cover product has been used. These four studies help synthesized, at nominal 1 km, to obtain a consensus cropland mask of the world (global

cropland extent version 1.0 or GCE V1.0). It was demonstrated from these products that the uncertainty in location of croplands in any one given product is quite high and no single product maps croplands particularly well. Therefore, a synthesis identifies where some or all of these products agree and where they disagree. This provides a starting point for the next level of more detailed cropland mapping at 250 and 30 m (see ongoing efforts at: http://geography.wr.usgs.gov/science/croplands/ and https://www.croplands.org/). The five key cropland products identified to be derived from remote sensing are: (1) cropland extent\areas, (2) cropping intensities, (3) watering method (irrigated versus rain-fed), (4) crop type, and (5) cropland change over time and space. From these primary products, one can derive crop productivity and water productivity. Such products have great importance and relevance in global food security analysis.

Authors recommend the use of composite global cropland map (see Figure 6.12c; Table 6.7c) that provides clear consensus view on of four major cropland studies on global

- Cropland extent location
- Cropland watering method (irrigation versus rain-fed)

The nominal 1 km product (Figure 6.12c and Table 6.7c) does not show where the crop types are or even where the crop dominance occur. However, cropping intensity can be generated using multitemporal remote sensing for every pixel over these cropland areas.

Acknowledgments

The authors thank NASA Making Earth Science Data Records for Use in Research Environments (MEaSUREs) solicitation for funding this research. Support by USGS Powell Center for a working group on global croplands is much appreciated. We thank the global food security support analysis data @ 30 m (GFSAD30) project team for inputs. Figures 6.1 and 6.2 were produced by Dr. Zhuoting Wu, USGS Mendenhall Post Doctoral Researcher, we thank her for it.

References

Biggs, T., Thenkabail, P. S., Krishna, M., GangadharaRao, P., and Turral, H. (2006). Vegetation phenology and irrigated area mapping using combined MODIS time-series, ground surveys, and agricultural census data in Krishna River Basin, India. *International Journal of Remote Sensing*, 27 (19), 4245–4266.

Bindraban, P. S., Bulte, E. H., and Conijn, S. G. (2009). Can large-scale biofuel production be sustained by 2020? *Agricultural Systems*, 101, 197–199.

Biradar, C. M., Thenkabail, P. S., Noojipady, P., Li, Y., Dheeravath, V., Turral, H., Velpuri, M. et al. (2009). A global map of rainfed cropland areas (GMRCA) at the end of last millennium using remote sensing. *International Journal of Applied Earth Observation and Geoinformation*, 11 (2), 114–129. doi:10.1016/j.jag.2008.11.002.

Chander, G., Markham, B. L., and Helder, D. L. (2009). Summary of current radiometric calibration coefficients for Landsat MSS, TM, ETM+, and EO-1 ALI sensors. *Remote Sensing of Environment*, 13 (5), 893–903. ISSN 0034-4257, http://dx.doi.org/10.1016/j.rse.2009.01.007. http://www.sciencedirect.com/science/article/pii/S0034425709000169. Last accessed March 15th, 2014.

Cohen, W. B. and Goward, S. N. (2004). Landsat's role in ecological applications of remote sensing. *BioScience*, 54, 535–545.

Congalton, R. (1991). A review of assessing the accuracy of classifications of remotely sensed data. *Remote Sensing of Environment*, 37, 35–46.

Congalton, R. (2009). Accuracy and error analysis of global and local maps: Lessons learned and future considerations. In: *Remote Sensing of Global Croplands for Food Security*, P. Thenkabail, J. Lyon, H. Turral, and C. Biradar (eds). CRC/Taylor & Francis, Boca Raton, FL, pp. 441–458.

Congalton, R. and Green, K. (2009). *Assessing the Accuracy of Remotely Sensed Data: Principles and Practices*, 2nd edn. CRC/Taylor & Francis, Boca Raton, FL, 183pp.

Crist, E. P. and Cicone, R. C. (1984). Application of the tasseled cap concept to simulated Thematic Mapper data. *Photogrammetric Engineering and Remote Sensing*, 50, 343–352.

DeFries, R., Hansen, M., Townsend, J. G. R., and Sohlberg, R. (1998). Global land cover classifications at 8 km resolution: The use of training data derived from Landsat imagery in decision tree classifiers. *International Journal of Remote Sensing*, 19, 3141–3168.

Dheeravath, V., Thenkabail, P. S., Chandrakantha, G, Noojipady, P., Biradar, C. B., Turral, H., Gumma, M. I., Reddy, G. P. O., and Velpuri, M. (2010). Irrigated areas of India derived using MODIS 500m data for years 2001–2003. *ISPRS Journal of Photogrammetry and Remote Sensing*, 65 (1), 42–59. http://dx.doi.org/10.1016/j.isprsjprs.2009.08.004.

EPW (2008). Food Security Endangered: Structural changes in global grain markets threaten India's food security. *Economic and Political Weekly*, 43, 5.

FAO (2009). *Food Outlook: Outlook Global Market Analysis*. Rome: FAO.

Foley, J. A., DeFries, R., Asner, G. P., Barford, C., Bonan, G., Carpenter, S. R., Chapin, F. S. et al. (2011). Solutions for a cultivated planet. *Nature*, 478 (7369), 337–342.

Foley, J. A., Monfreda, C., Ramankutty, N., and Zaks, D. (2007). Our share of the planetary pie. *PNAS*, 104, 12585–12586.

Falkenmark, M. and Rockström, J. (2006). The new blue and green water paradigm: Breaking new ground for water resources planning and management. *Journal of Water Resource Planning and Management*, 132, 1–15.

Friedl, M. A., McIver, D. K., Hodges, J. C. F., Zhang, X. Y., Muchoney, D., and Strahler, A. H. (2002). Global land cover mapping from MODIS: Algorithms and early results. *Remote Sensing of Environment*, 83, 287–302.

Friedl, M. A., Sulla-Menashe, D., Tan, B., Schneider, A., Ramankutty, N. S., and Huang, X. M. (2010). MODIS Collection 5 global land cover: Algorithm refinements and characterization of new datasets. *Remote Sensing of Environment*, 114 (1), 168–182.

Funk, C. and Brown, M. (2009). Declining global per capita agricultural production and warming oceans threaten food security. *Food Security*, 1 (3), 271–289. doi:10.1007/s12571–009–0026-y.

Gibbs, H. K., Johnston, M., Foley, J. A., Holloway, T., Monfreda, C., Ramankutty, N., and Zaks, D. (2008). Carbon payback times for crop-based biofuel expansion in the tropics: The effects of changing yield and technology. *Environment Research Letters*, 3(2008), 034001, 10pp. doi:10.1088/1748–9326/3/3/034001.

Goldewijk, K., Beusen, A., de Vos, M., and van Drecht, G. (2011). The HYDE 3.1 spatially explicit database of human induced land use change over the past 12,000 years. *Global Ecology and Biogeography*, 20 (1), 73–86. doi:10.1111/j.1466–8238.2010.00587.x.

Goodchild, M. and Gopal, S. (eds.) (1989). *The Accuracy of Spatial Databases*. Taylor & Francis, New York, 290pp.

Gordon, L. J., Finlayson, C. M., and Falkenmark, M. (2009). Managing water in agriculture for food production and other ecosystem services. *Agricultural Water Management*, 97, 512–519. doi: 10.1016/j.agwat.2009.03.017.

Gumma, M. K., Nelson, A., Thenkabail, P. S., and Singh, A. N. (2011). Mapping rice areas of South Asia using MODIS multi temporal data. *Journal of Applied Remote Sensing,* 5, 053547 (September 1, 2011). doi:10.1117/1.3619838.

Gutman, G., Byrnes, R., Masek, J., Covington, S., Justice, C., Franks, S., and Headley, R. (2008). Towards monitoring Land-cover and land-use changes at a global scale: The global land survey 2005. *Photogrammetric Engineering and Remote Sensing*, 74 (1): 6–10.

Hansen, M. C., DeFries, R. S., Townshend, J. R. G., Sohlberg, R., Dimiceli, C., and Carroll, M. (2002). Towards an operational MODIS continuous field of percent tree cover algorithm: Examples using AVHRR and MODIS data. *Remote Sensing of Environment,* 83, 303–319.

Hossain, M., Janaiah, A., and Otsuka, K. (2005). Is the productivity impact of the Green Revolution in rice vanishing? *Economic and Political Weekly* 5595–9600.

Jiang, Y. (2009). China's water scarcity. *Journal of Environmental Management*, 90, 3185–3196.

Johnson, D. M. and Mueller, R. (2010). The 2009 cropland data layer. *Photogrammetric Engineering and Remote Sensing*, 76 (11), 1201–1205.

Khan, S. and Hanjra, M. A. (2008). Sustainable land and water management policies and practices: A pathway to environmental sustainability in large irrigation systems. *Land Degradation and Development*, 19, 469–487.

Kumar, M. D. and Singh, O. P. (2005). Virtual water in global food and water policy making: Is there a need for rethinking? *Water Resources Management,* 19, 759–789.

Kurz, B. and Seelan, S. K. Use of remote sensing to map irrigated agriculture in areas overlying the Ogallala Aquifer, U.S. In Remote Sensing of Global Croplands for Food Security; Thenkabail, P. S., Turral, H., Lyon, J. G., Biradar, C., Eds.; CRC Press: Boca Raton, FL, 2009.

Lal, R. and Pimentel, D. (2009). Biofuels from crop residues. *Soil and Tillage Research*, 93, 237–238.

Loveland, T. R., Reed, B. C., Brown, J. F., Ohlen, D. O., Zhu, Z., and Yang, L. (2000). Development of global land cover characteristics database and IGBP DISCover from 1 km AVHRR data. *International Journal of Remote Sensing*, 21, 1303–1330.

McIntyre, B. D. (2008). International assessment of agricultural knowledge, science and technology for development (IAASTD): Global report. Includes Bibliographical References and Index. ISBN 978-1-59726-538-6, Oxford, U.K.

Masek, J. G., Huang, C., Wolfe, R., Cohen, W., Hall, F., Kutler, J., and Nelson, P. (2008). North American forest disturbance mapped from a decadal Landsat record. *Remote Sensing of Environment,* 112, 2914–2926.

Masek, J. G., Vermote, E. F., Saleous, N., Wolfe, R., Hall, F. G., Huemmrich, Gao, F., Kutler, J., and Lim, T. K. (2006). A Landsat surface reflectance data set for North America, 1990–2000. *Geoscience and Remote Sensing Letters,* 3, 68–72.

Monfreda, C., Patz, J. A., Prentice, I. C., Ramankutty, N., and Snyder, P. K. (2005). Global consequences of land use. *Science* July 22; 309 (5734), 570–574.

Monfreda, C., Ramankutty, N., and Foley, J. A. (2008). Farming the planet: 2. Geographic distribution of crop areas, yields, physiological types, and net primary production in the year 2000. *Global Biogeochemical Cycles* 22 (1), GB1022.

Olofsson, P., Stehman, S. V., Woodcock, C. E., Sulla-Menashe, D., Sibley, A.M., Newell, J.D. et al. (2012). A global land cover validation dataset, I: Fundamental design principles. *International Journal of Remote Sensing*, 33, 5768–5788.

Ozdogan, M. and Gutman, G. (2008). A new methodology to map irrigated areas using multi-temporal MODIS and ancillary data: An application example in the continental US. *Remote Sensing of Environment,* 112 (9), 3520–3537.

Ozdogan, M. and Woodcock, C. E. (2006). Resolution dependent errors in remote sensing of cultivated areas. *Remote Sensing of Environment,* 103, 203–217.

Pennisi, E. (2008). The Blue revolution, drop by drop, gene by gene. *Science,* 320 (5873): 171–173. doi:10.1126/science.320.5873.171

Pittman, K., Hansen, M. C., Becker-Reshef, I., Potapov, P. V., and Justice, C. O. (2010). Estimating global cropland extent with multi-year MODIS data. *Remote Sensing* 2 (7), 1844–1863.

Portmann, F., Siebert, S., and Döll, P. (2010). MIRCA2000—Global monthly irrigated and rainfed crop areas around the year 2000: A new high-resolution data set for agricultural and hydrological modelling. *Global Biogeochemical Cycles*, 24 GB0003435. 24pp.

Ramankutty, N., Evan, A. T., Monfreda, C., and Foley, J. A. (2008). Farming the planet: 1. Geographic distribution of global agricultural lands in the year 2000. *Global Biogeochemical Cycles,* 22. 19pp. doi:10.1029/2007GB002952.

Ramankutty, N. and Foley, J. A. (1998). Characterizing patterns of global land use: An analysis of global croplands data. *Global Biogeochemical Cycles* 12 (4), 667–685.

Rodell, M., Velicogna, I., and Famiglietti, J. S. (2009). Satellit-based estimates of groundwater depletion in India. *Nature,* 460, 999–1002. doi:10.1038/nature08238.

Sakamoto, T., Yokozawa, M., Toritani, H., Shibayama, M., Ishitsuka, N., Ohno, H. (2005), A crop phenology detection method using time-series MODIS data. *Remote Sensing of Environment*, 96, 366–374.

Searchinger, T., Heimlich, R., Houghton, R. A., Dong, F., Elobeid, A., Fabiosa, J., Tokgoz, S., Hayes, D., and Yu, T. H. (2008). Use of U.S. croplands for biofuels increases greenhouse gases through emissions from land-use change. *Science,* 319, 1238–1240.

Siebert, S. and Döll, P. (2010). Quantifying blue and green virtual water contents in global crop production as well as potential production losses without irrigation. *Journal of Hydrology*. 384(3–4), 198–217. doi:10.1016/j.jhydrol.2009.07.031.

Siebert, S., Hoogeveen, J., and Frenken, K. (2006). *Irrigation in Africa, Europe and Latin America—Update of the digital global map of irrigation areas to version 4*, Frankfurt Hydrology Paper 05, 134 pp. Institute of Physical Geography, University of Frankfurt, Frankfurt am Main, Germany and Rome, Italy.

Thenkabail, P. S., Biradar, C. M., Noojipady, P., Cai, X. L., Dheeravath, V., Li, Y. J., Velpuri, M., Gumma, M., and Pandey, S. (2007b). Sub-pixel irrigated area calculation methods. *Sensors Journal* (special issue: Remote Sensing of Natural Resources and the Environment (Remote Sensing Sensors Edited by Assefa M. Melesse). 7: 2519–2538. http://www.mdpi.org/sensors/papers/s7112519.pdf.)

Thenkabail, P. S., Biradar, C. M., Noojipady, P., Dheeravath, V., Li, Y. J., Velpuri, M., Gumma, M. et al. (2009b). Global irrigated area map (GIAM), derived from remote sensing, for the end of the last millennium. *International Journal of Remote Sensing*, 30 (14), 3679–3733. July, 20, 2009.

Thenkabail, P. S., Enclona, E. A., Ashton, M. S., Legg, C., Jean De Dieu, M. (2004). Hyperion, IKONOS, ALI, and ETM+ sensors in the study of African rainforests. *Remote Sensing of Environment*, 90, 23–43.

Thenkabail, P. S., GangadharaRao, P., Biggs, T., Krishna, M., and Turral, H., (2007a). Spectral matching techniques to determine historical land use/land cover (LULC) and irrigated areas using time-series AVHRR pathfinder datasets in the Krishna river Basin, India. *Photogrammetric Engineering and Remote Sensing*, 73 (9), 1029–1040. (Second Place Recipients of the 2008 John I. Davidson ASPRS President's Award for Practical papers).

Thenkabail, P. S., Hanjra, M. A., Dheeravath, V., Gumma, M. (2011). Global croplands and their water use remote sensing and non-remote sensing perspectives. In: Weng, Q. (ed.), *Advances in Environmental Remote Sensing: Sensors, Algorithms, and Applications*, Taylor & Francis, pp. 383–419.

Thenkabail, P. S., Hanjra, M. A., Dheeravath, V., Gumma, M. A. (2010). A holistic view of global croplands and their water use for ensuring global food security in the 21st century through advanced remote sensing and non-remote sensing approaches. *Journal Remote Sensing*, 2 (1), 211–261. doi:10.3390/rs2010211. http://www.mdpi.com/2072–4292/2/1/211.

Thenkabail, P. S., Knox, J. W., Ozdogan, M., Gumma, M. K., Congalton, R. G., Wu, Z., Milesi, C. et al. (2012). Assessing future risks to agricultural productivity, water resources and food security: How can remote sensing help? *Photogrammetric Engineering and Remote Sensing*, August 2012 Special Issue on Global Croplands: Highlight Article. 78(8), 773–782.

Thenkabail, P. S., Lyon, G. J., Turral, H., and Biradar, C. M. (2009a). *Remote Sensing of Global Croplands for Food Security.* CRC Press-Taylor & Francis group, Boca Raton, FL, London, New York. pp. 556 (48 pages in color). Published in June, 2009.

Thenkabail, P. S., Lyon, G. J., Turral, H., and Biradar, C. M. (2009c). *Remote Sensing of Global Croplands for Food Security*. Boca Raton, FL, London, New York: CRC Press/Taylor & Francis Group, Published in June.

Thenkabail, P. S., Mariotto, I., Gumma, M. K., Middleton, E. M., Landis, and D. R., Huemmrich, F. K. (2013). Selection of hyperspectral narrowbands (HNBs) and composition of hyperspectral twoband vegetation indices (HVIs) for biophysical characterization and discrimination of crop types using field reflectance and Hyperion/EO-1 data. *IEEE Journal of Selected Topics in Applied Earth Observations and Remote Sensing* 6 (2), 427–439, April 2013. doi:10.1109/JSTARS.2013.2252601.

Thenkabail, P. S., Schull, M., and Turral, H. 2005. Ganges and Indus River Basin Land Use/Land Cover (LULC) and irrigated area mapping using continuous streams of MODIS data. *Remote Sensing of Environment*, 95 (3), 317–341.

Thenkabail, P. S. and Wu, Z. (2012). An automated cropland classification algorithm (ACCA) for Tajikistan by combining landsat, MODIS, and secondary data. *Remote Sensing,* 4 (10), 2890–2918.

Tillman, D., C. Balzer, J. Hill, and B. L. Befort, 2011. Global food demand and the sustainable intensification of agriculture, *Proceedings of the National Academy of Sciences of the United States of America*, November 21. doi:10.1073/pnas.1116437108. Tomlinson, R. 2003. Thinking about Geographic Information Systems Planning for Managers, 283 ESRI Press.

Turral, H., Svendsen, M., and Faures, J. (2009). Investing in irrigation: Reviewing the past and looking to the future. *Agricultural Water Management*. 97(2010), 551–560. doi:101.1016/j.agwt.2009.07.012.

UNDP (2012). *Human Development Report 2012: Overcoming Barriers: Human Mobility and Development*. New York: United Nations.

Velpuri, M., Thenkabail, P. S., Gumma, M. K., Biradar, C. B., Dheeravath, V., Noojipady, P., and Yuanjie, L. (2009). Influence of resolution or scale in irrigated area mapping and area estimations. *Photogrammetric Engineering and Remote Sensing* (PE&RS). 75 (12), December 2009, 1383–1395.

Vinnari, M. and Tapio, P. (2009). Future images of meat consumption in 2030. *Futures*, 41 (5), 269–278. doi:10.1016/j.futures.2008.11.014.

Wada, Y., van Beek, L. P. H., and Bierkens, M. F. P. (2012). Nonsustainable groundwater sustaining irrigation: A global assessment. *Water Resources Research*, 48, W00L06. doi:10.1029/2011WR010562.

Wardlow, B. D. and Egbert, S. L. (2008). Large-area crop mapping using time-series MODIS 250 m NDVI data: An assessment for the U.S. Central Great Plains. *Remote Sensing of Environment*, 112, 1096–1116.

Wardlow, B. D., Egbert, S. L., and Kastens, J. H. (2007). Analysis of time-series MODIS 250 m vegetation index data for crop classification in the U.S. Central Great Plains. *Remote Sensing of Environment*, 108, 290–310.

Wardlow, B. D., Kastens, J. H., and Egbert, S. L. (2006). Using USDA crop progress data for the evaluation of greenup onset date calculated from MODIS 250-meter data. *Photogrammetric Engineering and Remote Sensing*, 72, 1225–1234.

Wu, Z., Thenkabail, P. S., and Verdin, J. (2014b). An automated cropland classification algorithm (ACCA) using Landsat and MODIS data combination for California. *Photogrammetric Engineering and Remote Sensing,* 80 (1): 81–90.

Wu, Z., Thenkabail, P. S., Zakzeski, A., Mueller, R., Melton, F., Rosevelt, C., Dwyer, J., Johnson, J., and Verdin, J. P. (2014a). Seasonal cultivated and fallow cropland mapping using modis-based automated cropland classification algorithm. *Journal of Applied Remote Sensing* 0001;8 (1), 083685. doi:10.1117/1.JRS.8.083685.

Yu, L., Wang, J., Clinton, N., Xin, Q., Zhong, L., Chen, Y., and Gong, P. (2013). FROM-GC: 30 m global cropland extent derived through multisource data integration. *International Journal of Digital Earth.* 12pp. doi:10.1080/17538947.2013.822574.